11-30-2018

Optimization of Bacterial Expression and Purification of Nipsnap1 Protein

Jay Michael Yarbro

OPTIMIZATION OF BACTERIAL EXPRESSION AND PURIFICATION OF Nipsnap1 PROTEIN

by

Jay Michael Yarbro

A Thesis

Submitted in Partial Fulfillment of the

Requirements for the Degree of

Master of Science

Major: Chemistry

The University of Memphis

December 2018

Abstract

Nipsnap1 (4-nitrophenylphosphatase domain and non-neuronal SNAP25-like homolog 1) is a novel mitochondrial protein shown to interact with the intracellular domain of amyloid precursor protein (APP), one of the key biomarkers implicated in Alzheimer's disease (AD) pathology. A formerly developed expression strategy for Nipsnap1 based on the pET-28a expression system showed direct binding of purified recombinant Nipsnap1 to NAD+ and NADP+. This was further confirmed using Circular Dichroism (CD) spectroscopy, indicating that NAD+ binding produces a structural change in Nipsnap1.

To address the low yield of Nipsnap1 protein in the former expression system, several approaches and conditions were evaluated in this study. A GST-fusion strategy was developed to stabilize the recombinant protein. GST fusion did not result in sufficient solubility of Nipsnap1, with the majority of expressed GST-fused Nipsnap1 aggregating in inclusion bodies. Growth curve analysis showed that Nipsnap1 expression did not cause a bacteriostatic effect. After several experiments to optimize induction, solubilization and purification of recombinant Nipsnap1, the yield for Nipsnap1 remained low, but several truncated forms of Nipsnap1 were expressed in higher quantities. Future strategies of recombinant Nipsnap1 expression and purification may benefit from the use of a codon-optimized form of Nipsnap1 introduced into expression systems known to aid in protein solubility and stability.

TABLE OF CONTENTS

List of tables v

List of figures vi

Key to abbreviations ix

I - INTRODUCTION AND BACKGROUND 1

Alzheimer's disease 1
Amyloid precursor protein 2
Nipsnap1 is an APP-interacting protein 3
Evolutionary conservation of the Nipsnap1 C-terminus and the Nipsnap family 4
The structure and functions of Nipsnap1 are unknown 6
Insight into Nipsnap1 function 12
Significance 16
Project Goals 19

II – METHODS 20

Initial expression, purification, and analysis Nipsnap1-FL using pET-28a expression system 20
Nipsnap1 expression and optimization using pGEX-4T1 vector 21
Bacterial culture and growth curve preparation 27
Initial pGEX-4T1 Nipsnap1 expression and purification 28
Optimization of Nipsnap1 induction 30
Optimization of Nipsnap1 solubilization 32
Optimization of Nipsnap1 elution 34
Large-scale Nipsnap1 expression and purification 35

III – RESULTS 36

CD spectroscopy indicates NAD+ causes a structural shift in Nipsnap1 36
Nipsnap1 expression does not affect growth of BL21(DE3)pLysS Cells 37
Initial parameters for Nipsnap1 purification were not optimal 40
Optimization of Nipsnap1 induction 41
Optimization of Nipsnap1 solubilization 47

Large-scale expression with optimized lysis and purification results in truncated Nipsnap1 proteins 50

IV –DISCUSSION 54

REFERENCES 60

APPENDIX 67

List of Tables

Table 1. Overview of the four Nipsnap homologues in human. 6

Table 2. Primers used to introduce Nipsnap1 into pGEX-4T1. 23

Table 3. Summary of predicted sizes for Nipsnap1 cDNA and protein. 26

Table 4. Buffers used in GST-based protein purification. 29

Table 5. Summary of conditions used in comparison of 18 °C and 37 °C induction. 32

Table 6. Comparison of initial and final solubilization protocols. 34

List of Figures

Figure 1. Sequence alignment of the four Nipsnap homologues in mouse. 5

Figure 2. Sequence alignment of Nipsnap1 proteins from *Rhizobium radiobacter*, zebrafish, mouse, and human. 7

Figure 3. Nipsnap 1 as shown in the UCSC Genome Browser on C. elegans Feb. 2013 (WBcel235/ce11) Assembly. 8

Figure 4. Human Nipsnap1 gene expression across tissues from GTEx. 10

Figure 5. Crystal structure of a NIPSNAP protein from *Agrobacterium tumefacience*. 10

Figure 6. Alignment of the structure model generated by FINDSITEcomb of the C-terminal fragment of Nipsnap1 to experimental NIPSNAP domain structures. 13

Figure 7. Comparison of Nipsnap1 structural models generated by I-TASSER and FINDSITEcomb. 15

Figure 8. Sequence alignment of the NIPSNAP domain containing fragments of Nipsnap1 with sequences of NIPSNAP proteins with experimental structures. 15

Figure 9. Reduction in NAD/NADH ratio in Nipsnap1 deficient mice. 17

Figure 10. Biochemical pull-down using NAD(P). 18

Figure 11. Diagram showing approach to developing a recombinant Nipsnap1 purification system using the pGEX plasmid. 22

Figure 12. Plasmid map of the pGEX-4T1 plasmid. 24

Figure 13. Design map for the three Nipsnap1 constructs developed. 25

Figure 14. Nipsnap1 cDNAs generated via PCR amplification. 26

Figure 15. Schematic of bacterial growth curve experimentation. 27

Figure 16. Workflow of GST purification strategy. 30

Figure 17. Circular dichroism spectra for Nipsnap1, NAD+, and Nipsnap1 in the presence of NAD+. 37

Figure 18. Bacterial growth curves generated pGEX-4T1 transformed cells. 39

Figure 19. Coomassie stain showing initial attempt at purification. 40

Figure 20. Coomassie stain of induced samples and control. 42

Figure 21. NTF Nipsnap1 expression in bacterial cultures induced with varying IPTG concentrations and grown for different times visualized by Coomassie. 44

Figure 22. Temperature effect on protein expression. 46

Figure 23. Coomassie stain comparing solubilization procedures using lysozyme or NP40. 48

Figure 24. Comparison of Nipsnap1-CTF solubilization using initial and final sonication methods. 49

Figure 25. Coomassie staining of samples from purification of supernatants generated from cultures transformed with empty pGEX-4T1 or pGEX-4T1 encoding CTF Nipsnap1. 51

Figure 26. Western blot analysis of samples from purification of supernatants generated from cultures transformed with empty pGEX-4T1 or pGEX-4T1 encoding CTF Nipsnap1. 52

Figure 27. Nipsnap1 cDNA sequence used to generate full-length Nipsnap1. 57

Key to Abbreviations

ABAD – Aβ-binding alcohol dehydrogenase

AD – Alzheimer's disease

AICD – APP intracellular domain

APP – Amyloid precursor protein

Aβ – Amyloid-beta

CD – Circular Dichroism

CTF – C-terminal fragment Nipsnap1

CypD – Cyclophilin D

FL – full-length Nipsnap1

GST – Glutathione S-transferase

IPTG - Isopropyl β-D-1-thiogalactopyranoside

ITC – Isothermal calorimetry

NAD+ - Nicotinamide adenine dinucleotide, oxidized

NADH – Nicotinamide adenine dinucleotide, reduced

NADP+ - Nicotinamide adenine dinucleotide phosphate, oxidized

NADPH – Nicotinamide adenine dinucleotide phosphate, reduced

Nipsnap1 - 4-nitrophenylphosphatase domain and non-neuronal SNAP25-like homolog 1

NTF – N-terminal fragment Nipsnap1

SDS-PAGE - Sodium dodecyl sulfate–polyacrylamide gel electrophoresis

Tm – Melting temperature

TOM22 - Mitochondrial chaperone translocase of the outer membrane 22

I – INTRODUCTION AND BACKGROUND

Alzheimer's disease

Alzheimer's disease (AD) is a progressive neurodegenerative disease and the most common cause of dementia (Wilson 2012; Barker 2002), a group of symptoms that begins with deterioration in memory (Reitz 2011), with an eventual decline in language and cognitive functionality and skills. AD is the 6th leading cause of death in the United states, currently affecting 5.7 million Americans over the age of 65 (alz.org) and is projected to grow to 88 million by 2050 (He 2016; US Census Bureau 2014). Current estimates state that AD and other dementias will cost the US $277 billion, with projected costs to rise as high as $1.1 trillion by 2050. Early and accurate diagnosis could save up to $7.9 trillion in medical care and costs (alz.org)

There is currently no definitive test for AD diagnosis. Physicians currently rely on several tools and assessments to make a differential diagnosis, including cognitive tests, neurological examinations, brain imaging, and obtaining the medical and family history of the individual (alz.org)

AD pathology is characterized by the accumulation of two proteins, including an abnormal form of the tau protein (tau tangles) inside of neurons, and the protein fragment amyloid-beta (Aβ) outside of neurons. Additional hallmarks of AD pathology include chronic inflammation, loss of neuronal connections and cell death, and numerous vascular issues (nia.nih.gov).

Amyloid precursor protein

Amyloid precursor protein (APP) is a single pass transmembrane protein and is a member of the APP family of proteins, including amyloid precursor-like protein 1 (APLP1) and amyloid precursor-like protein 2 (APLP2) (Zhang 2011), which play essential but redundant roles during development (Heber 2000). The APP family of proteins are expressed in the developing and mature brain at the somal cell surface along growing axons and at the axonal growth cone (Selkoe 2002). APP is primarily processed within the Aβ sequence by α-secretase, releasing a soluble fragment known as APPS-α. This fragment has been shown to regulate APP function in neurite outgrowth through competition for the binding of integrin β with APP (Younge-Pearse 2008). Secreted forms of APP formed via α-secretase processing have been shown to have neurotrophic and neuroprotective properties via stabilization of the intraneuronal concentration of calcium (Mattson 1993).

APP can additionally undergo processing by β-secretase and γ-secretase. When aberrant processing of APP occurs by β-secretase, 40-42 amino acid (AA) long fragments of Aβ aggregate to form Aβ plaques. Mutations in APP that result in an increase of this aberrant processing is associated with some early onset forms of AD (Murrell 1991). Aβ plaques are neurotoxic through an interaction with Aβ-binding alcohol dehydrogenases (ABAD) and cyclophilin D (CypD), resulting in large-scale neuronal death over time. Aβ can induce apoptosis in cultured neurons directly by lipid peroxidation (Loo 1993). The remaining 83 AA long fragment of APP untouched after β-secretase cleavage can further be processed by γ-secretase, resulting in further cleavage and generation of the amyloid precursor protein intracellular domain (AICD). The AICD has been shown to induce

significant changes in gene expression and neuron-specific apoptosis, suggesting APP may be involved in signaling closely linked to AD pathology, and suggests a correlation in gene expression in neuron specificity of AICD-induced cell death (Nagase 2014; Ohkawara 2011). The AICD has furthermore been shown to induce neurotoxicity in rat primary cortical neurons by upregulating glycogen synthase kinase 3β (GSK-3β) expression and increasing tau phosphorylation (Kim 2003), one of the hallmarks of AD pathology that is highly correlated with dementia (Wang 2013).

Nipsnap1 is an APP-interacting protein

Previous work in our laboratory showed that the AICD interacts with the novel protein 4-Nitrophenylphosphatase Domain and Non-Neuronal SNAP25-Like Homolog 1 (Nipsnap1) using a functional proteomics approach (Tummala 2010). A synthetic peptide corresponding to APLP1 C-terminus or a randomized control peptide were cross-linked to an agarose resin and used for affinity chromatography. Mouse brain lysate was passed through the columns, and bound proteins were further separated by sodium dodecylsulfate polyacrylamide gel electrophoresis (SDS-PAGE), and visualized by silver staining, where a ~30 kDa protein was identified. The protein was trypsin-digested and subsequently sequenced using mass spectrometry. The molecular masses of 11 derived peptides were determined by matrix-assisted laser desorption／ionization time-of-flight mass spectrometry and used to search the non-redundant protein databases at NCBI. The protein was identified as Nipsnap1 (NM_008698) with approximately 40% sequence coverage. The protein was additionally found to be targeted to mitochondria via an N-

terminal mitochondrial targeting sequence and shown to interact with mitochondrial chaperone translocase of the outer membrane 22 (TOM22).

Evolutionary conservation of the Nipsnap1 C-terminal domain

Nipsnap1 belongs to a family of four genes (Table 1): Nipsnap1, Nipsnap2 (also known as GBAS), Nipsnap3 (also known as Nipsnap3B) and Nipsnap4 (also known as Nipsnap3A and TassC). Mitoprot analysis (Claros 1995) predicts that all four family members of the Nipsnap family have mitochondrial targeting sequences. Among the four Nipsnap proteins, Nipsnap1 and 2 share high sequence identity (75% identity of 245 residues overlap). An alignment of the four Nipsnap proteins in mouse is shown in Figure 1.

Figure 1. Sequence alignment of the four Nipsnap homologues in mouse. Alignment was generated using Clustal Omega 1.2.4 (Goujon 2010, Sievers 2011). Fully (*), strongly (:), and weakly (.) conserved residues are noted. Higher conservation of residues can be seen towards the C-terminus of the protein.

Table 1. Overview of the four Nipsnap homologues. Alternative names found in literature, human chromosomal locations (Casper 2018), tissues of highest expression, and the number of total amino acids in each homolog are shown.

Gene	Alternative Names	Location (hg38)	Highest Expression	Amino Acids
Nipsnap1		chr22:29,554,808-29,581,337	Liver, brain	284
Nipsnap2	GBAS	chr7:55,964,581-56,000,181	Brain, muscle	286
Nipsnap3A	Nipsnap4, TassC	chr9:104,747,688-104,760,122	Testis, fetal brain	247
Nipsnap3B	Nipsnap3	chr9:104,764,170-104,774,010	Skeletal muscle, testis	247

The structure and functions of Nipsnap1 are unknown

Nipsnap1 is an evolutionarily conserved protein found in a wide range of species including plants, *C. elegans*, zebrafish, mouse and human, with high sequence conservation stretching back to bacteria (Figure 2). However, the name Nipsnap1 (4 nitrophenyl phosphatase and non-neuronal SNAP25 like protein homolog1) is a misnomer; the protein has no known phosphatase or SNAP25 like domain or function. The protein is called Nipsnap1 due to it being found in the *C. elegans* operon present between the genes similar to yeast nitrophenyl phosphatase (cosmid K02D10 acc. L14710) (Sulston 1992) and mouse synaptosomal associated protein 29 (SNAP29) (Figure 3).

Human Nipsnap1 was characterized and found to be localized on chromosome 22q12 (Seroussi 1998). It was found that the gene had 10 exons which coded for a 284 amino acid protein and contained an unusual TATA-less GC-rich promoter sequence. Although there is limited knowledge pertaining to the structure and function of Nipsnap1, the gene exhibits widespread tissue expression in human and mouse, with highest levels

of expression in the liver and kidneys. Moderate expression is seen across nervous tissue, predominantly in the frontal cortex (Figure 4).

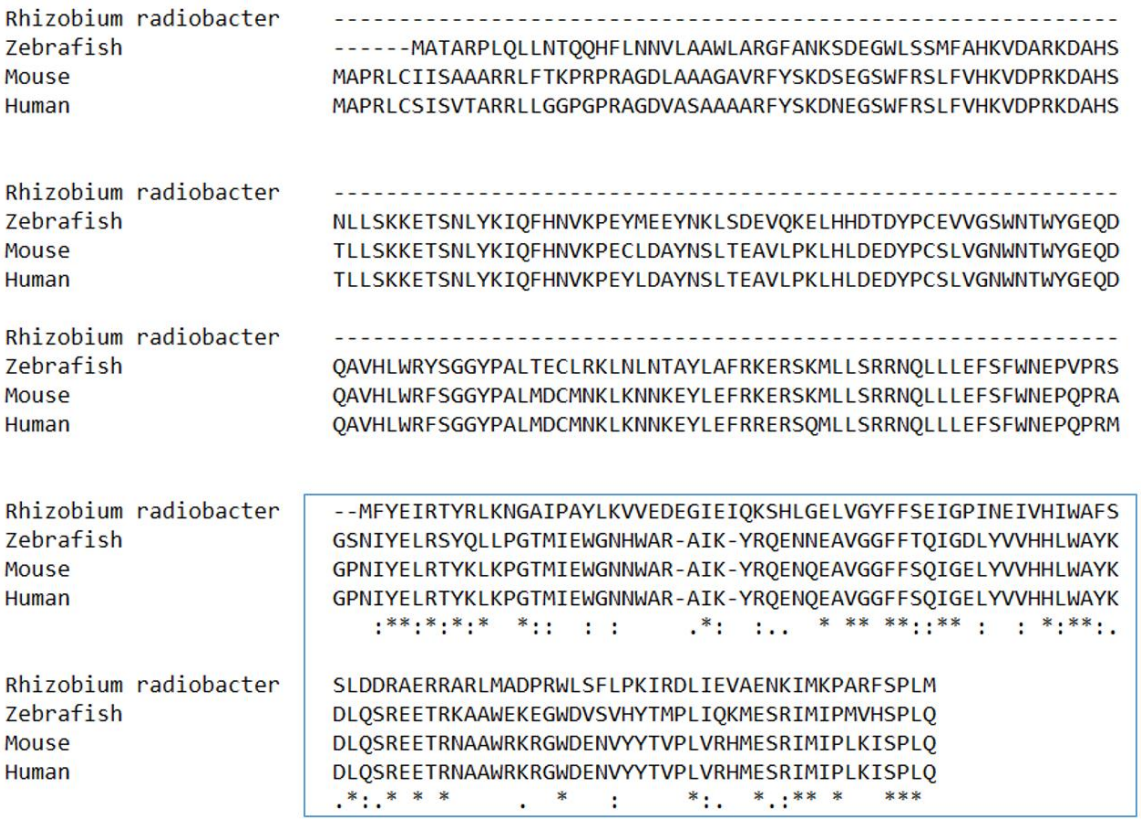

Figure 2. Sequence alignment of Nipsnap1 proteins from *Rhizobium radiobacter*, zebrafish, mouse, and human. Alignment was generated using Clustal Omega 1.2.4 (Goujon 2010, Sievers 2011). Fully (*), strongly (:), and weakly (.) conserved residues are noted. High conservation of residues spanning through evolutionary divergent species can be seen towards the C-terminus of the protein as highlighted.

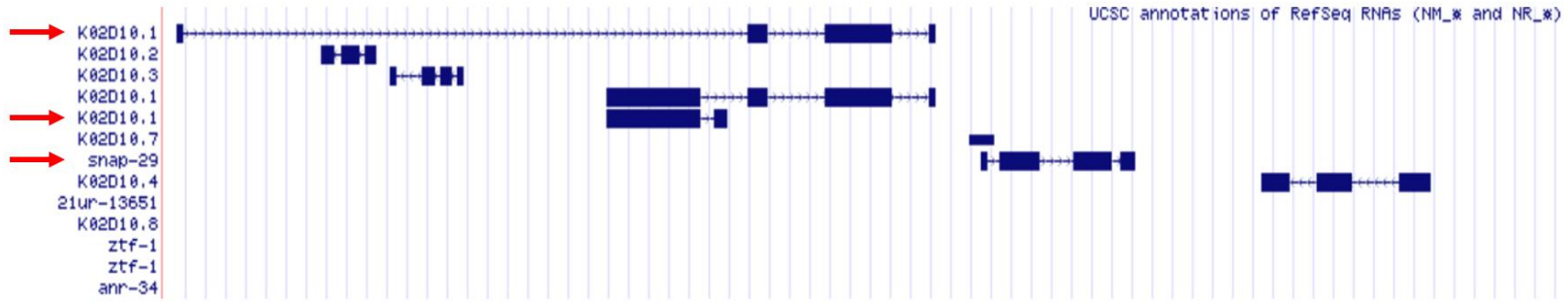

Figure 3. Nipsnap 1 (K02D10.1) as shown in the University of California Santa Cruz (UCSC) Genome Browser on C. elegans Feb. 2013 (WBcel235/ce11) Assembly (Howe 2016). The mammalian protein is called Nipsnap1 due to it having strong sequence similarity to a hypothetical protein found in the *C. elegans* operon (Sulston 1992) present between the genes similar to yeast nitrophenyl phosphatase (K02D10.1) and mouse synaptosomal associated protein 29 (SNAP29) on chromosome III. Relevant genes are noted with arrows.

There is no mammalian Nipsnap crystal structure available to date. However, crystal structures for Nipsnap proteins of certain agrobacterium such as *Agrobacterium tumefacience* do exist (Figure 5) (unpublished data from PDB database, Joint Center for Structural Genomics 2005). Structures are available for hypothetical protein atu4242 (1VQS) and atu5224 (1VQY) from *Agrobacterium tumefaciens* at 1.50 Å and 2.40 Å resolutions, respectively. Another crystal structure is available for atu4242 (2AP6). The data were deposited by the Joint Center for Structural Genomics and Northeast Structural Genomics Consortium. In rat liver mitochondria, Nipsnap1 (apparent mass 29 kDa) was identified as a complex with an apparent mass of 100−120 kDa, suggesting a homotrimeric assembly and/or association with another unidentified protein (Reifschneider 2006).

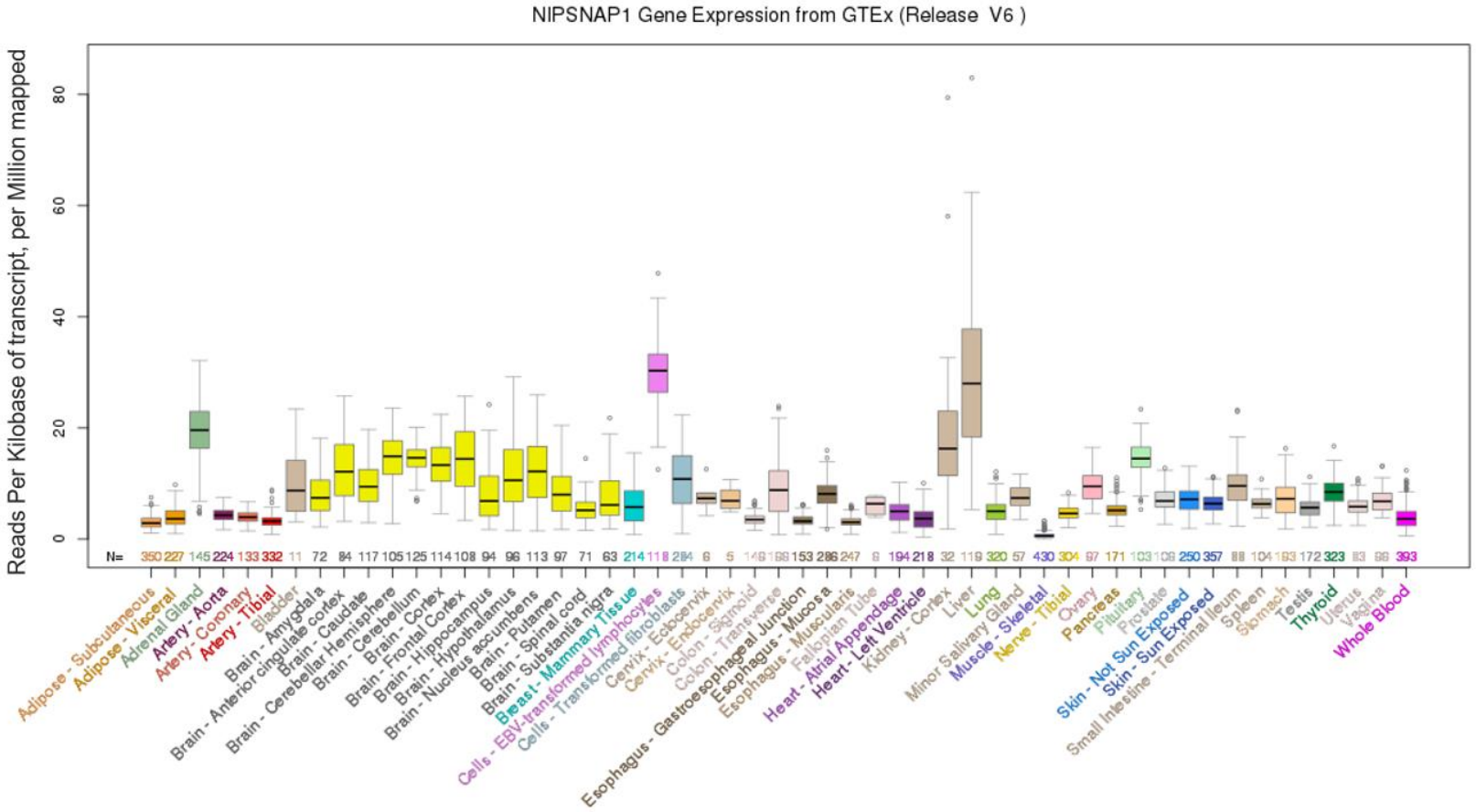

Figure 4. Human Nipsnap1 gene expression across tissues from Genotype-Tissue Expression project (GTEx) release V6 (GTEx Consortium, 2013). Highest Nipsnap1 expression is found in the liver, kidney, adrenal gland, and Epstein-Barr virus-transformed (EBV, herpes virus 4) lymphocytes. Moderate expression is seen across nervous tissue, predominantly in the frontal cortex.

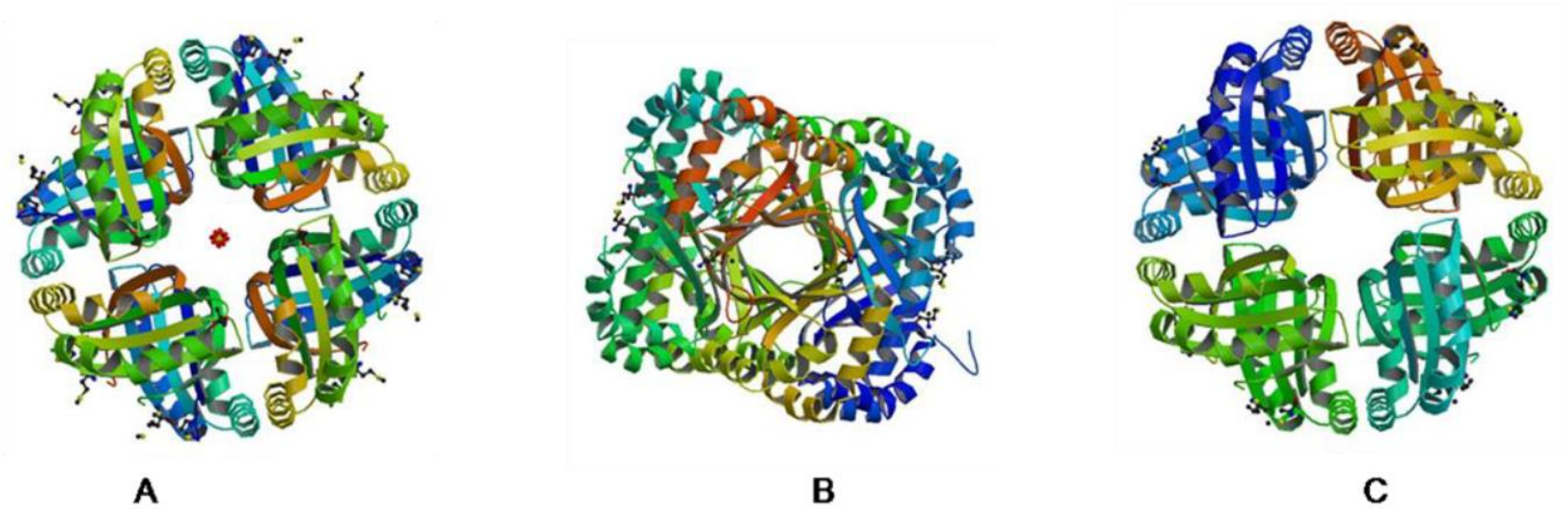

Figure 5. Crystal structure of a NIPSNAP protein from *Agrobacterium tumefacience*. (A) Biological Assembly Image for the crystal structure of a NIPSNAP family protein (atu4242) from *Agrobacterium tumefaciens* str. c58, 1VQS, at 1.50 Å resolution. (B) Biological assembly image for 1VQY, crystal structure of a NIPSNAP family protein (atu5224) from *Agrobacterium tumefaciens* str. c58 at 2.40 Å resolution. (A) and (B) were submitted by The Joint Center for Structural Genomics. (C) Biological assembly image for 2AP6, X-ray crystal structure of protein Atu4242 from *Agrobacterium tumefaciens*. The data was submitted by Benach J *et al.*, Northeast Structural Genomics Consortium. Data was acquired from the RCSB Protein Data Bank (Berman 2000), and the images generated by PISA and PQS (Goshal, unpublished).

Insight into Nipsnap1 function

Although little is known regarding Nipsnap1 function; protein distribution, screening/association studies and Nipsnap1 involvement in disease models have given some insights into its potential roles *in vivo*.

Gene expression analysis of heterozygous X-box binding protein 1 (XBP1) knockout mice showed that several genes on 11qA1 have altered expression, including strong upregulation of Nipsnap1 (Takata 2010). Nipsnap1 has been shown to inhibit transient receptor potential vanilloid channels 5 and 6 (TRPV5/6), Ca^{2+} ion channels expressed in mouse intestinal tissues (Schoeber 2008). Further evidence suggests Nipsnap1 has vital roles in the brain; an increase in Nipsnap1 expression was found in the postsynaptic density fraction (PSD) of mouse forebrains in a chemically induced epilepsy model (Satoh 2002), and changes in the PSD are believed to be vital in regulation of synaptic plasticity and important in learning and memory (Goelet 1986; Ehlers 2003).

Nipsnap1 was found to be expressed exclusively in neurons in mouse central nervous system (CNS), including pyramidal neurons in the cerebral cortex, Purkinje neurons in the cerebellum, and motor neurons in the spinal cord (Nautiyal 2010). Further work has determined Nipsnap1 can bind directly to the E2 subunit of pyruvate dehydrogenase in the branched chain amino acid (BCAA) metabolon (Islam 2010), suggesting a possible role for Nipsnap1in BCAA metabolism in mitochondria. Nipsnap1 has also been found to interact with the neuropeptide nocistatin (NST) and may play a role in pain transmission (Okuda-Ashitaka 2012) via mediating NST in inhibition of nociception/orphanin FQ (N/OFQ)-evoked tactile pain allodynia (Okuda-Ashitaka 2015). Nociceptive behavioral response increased in phase II of the formalin test (Hunskaar

1987) in Nipsnap1 deficient mice, suggesting that alteration of Nipsnap1 expression contributes to the pathogenesis of inflammatory pain (Okamoto 2016). Our group has shown that Nipsnap1 contains a mitochondrial targeting sequence at its N-terminus, and an interaction in its C-terminus with the C-terminal region of amyloid precursor protein (APP), suggesting that Nipsnap1 may regulate mitochondrial function in neurons (Tummala 2010). To investigate the function of Nipsnap1, our group generated a knock-out (KO) mouse model. We showed that targeted deletion of Nipsnap1 resulted in significant changes in the levels of many intermediate metabolites, not just those associated with BCAA metabolism (Ghoshal 2014).

Metabolomic profiling of brain and liver tissues from Nipsnap1 deficient mice revealed significant differences in nucleotide intermediates and NAD+ precursors (Ghoshal 2014). Two structure-based virtual ligand screening tools, I-TASSER (Iterative Threading ASSEmbly Refinement) (Zhang 2008; Roy 2010; Yang 2015) and FINDSITEcomb (Zhou 2013), were used to investigate potential functional roles of Nipsnap1. As the structure of Nipsnap1 has not been determined experimentally, a homology model was developed (Figures 6-8) from existing bacterial NIPSNAP crystal structures and used in screening. I-TASSER uses a hierarchical approach to predict protein structure and function, by identifying PDB templates using a multiple threading approach. Findsite performs ligand screening based on binding site conservation across evolutionary distant proteins identified by threading.

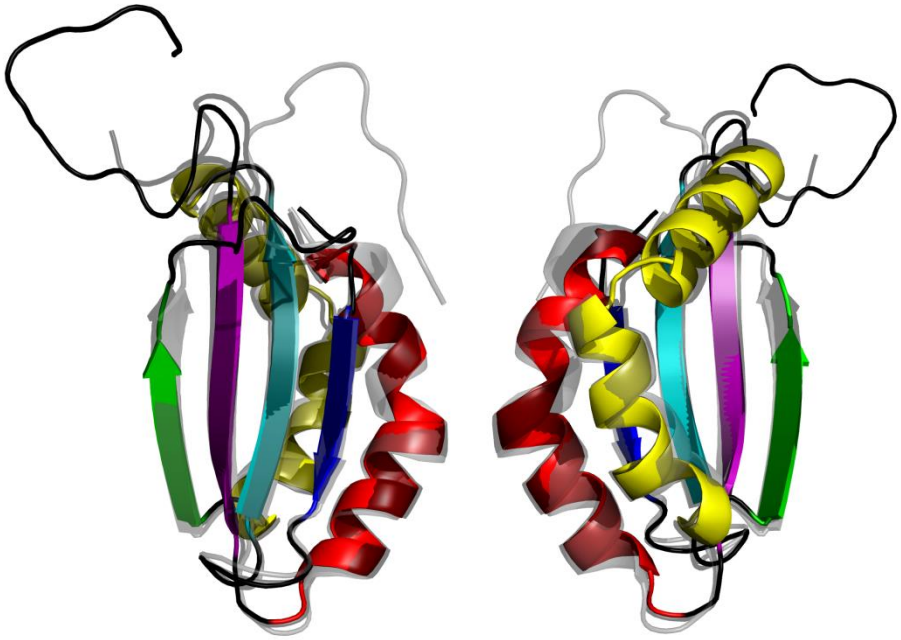

Figure 6. Alignment of the structure model generated by FINDSITEcomb of the C-terminal fragment of Nipsnap1 to experimental NIPSNAP domain structures (PDB codes 1VQS and 1VQY, shown in grey) (Joint Center for Structural Genomics 2005). The model of this fragment contains features of the NIPSNAP sequence domain previously defined by Seroussi et al. (Seroussi 1998)(Pfam ID PF07978) (Eberhardt 2016), including two α-helical regions from residues 195-215 (red) and 240-266 (yellow) and four β-strands involving residues 184-192 (purple), 218-222 (blue), 230-237 (teal), and 268-274 (green) (Ziebarth unpublished).

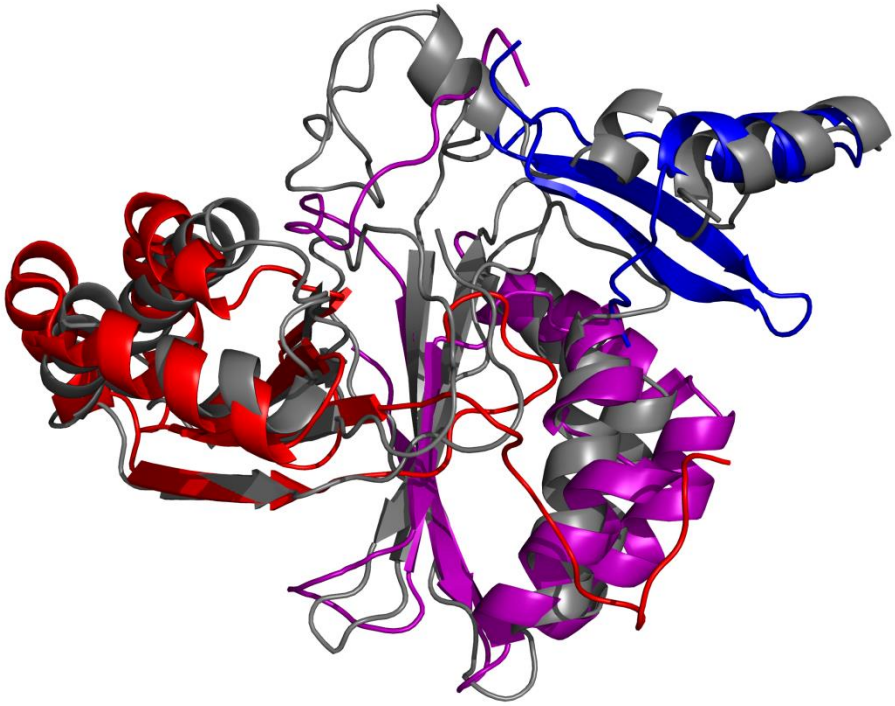

Figure 7. Comparison of Nipsnap1 structural models generated by I-TASSER and FINDSITEcomb. The I-TASSER model is shown in gray, while fragments 1, 2, and 3 of the FINDSITEcomb model are shown in blue, purple, and red, respectively. The image was created by superimposing the the FINDSITEcomb fragments to its corresponding sequence in the I-TASSER model (Ziebarth unpublished).

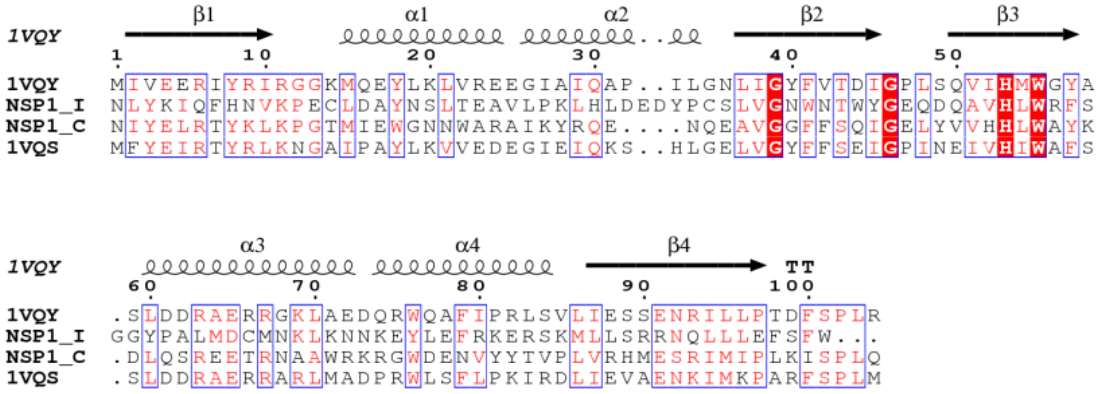

Figure 8. Sequence alignment of the NIPSNAP domain containing fragments of Nipsnap1 (NSP1_I and NPS1_C) with sequences of Nipsnap proteins with experimental structures (1VQS and 1VQY). Residues from the N-terminal end of the Nipsnap1 fragments NSP1_I and NSP1_C which did not align to the NIPSNAP domain were removed for clarity (Ziebarth unpublished).

Virtual ligand screening of Nipsnap1 identified NADH and NADPH as ligands that may bind to the NIPSNAP domain. FINDSITEcomb ranked NADH and NADPH as the two ligands most likely to bind out of a database of over 60,000 compounds. NADH was also in the top ~1% (734 out of 60,000) for binding to the entire Nipsnap1 protein. Systems genetics analysis of hippocampal tissue across a panel of recombinant inbred mouse strains revealed that Nipsnap1 expression tightly correlates with several dehydrogenases in addition to the previously reported PDH/BCKA dehydrogenases, including malate dehydrogenase, isocitrate dehydrogenase, and several NADH-Q reductase subunits.

Significance

Amyloid precursor protein (APP) is a type 1 transmembrane protein (Hynes 1990) whose mutant forms have been linked to Alzheimer's disease (AD) (Citron 1992; Murrell 1991). These mutations result in abnormal cleavage of APP and release of the APP intracellular domain (AICD) and amyloid beta (Aβ) peptide. Accumulating evidence suggests this cleavage results in some of the pathological features that are characteristic of AD (Muller 2008; Pimplikar 2010). The precise mechanism by which AICD is involved in normal and pathologic functions is unknown. An interaction has been described between a conserved region of AICD and the novel mitochondrial protein Nipsnap1 (Tummala 2010).

Taken together, these data suggest that Nipsnap1 may play an important role in mitochondrial function via regulation of NAD+/NADH levels. To test this hypothesis, enzymatic assays on brain tissues of Nipsnap1 deficient mice were performed, and it was

found that the NAD+/NADH ratio was significantly lower in Nipsnap1 deficient mice (Figure 9). These data have led to our central hypothesis that Nipsnap1 is an NAD+ binding protein that interacts with and regulates multiple dehydrogenase complexes in the mitochondria and that AICD, through a direct interaction with Nipsnap1, affects dehydrogenase activity and neuronal NAD+/NADH levels.

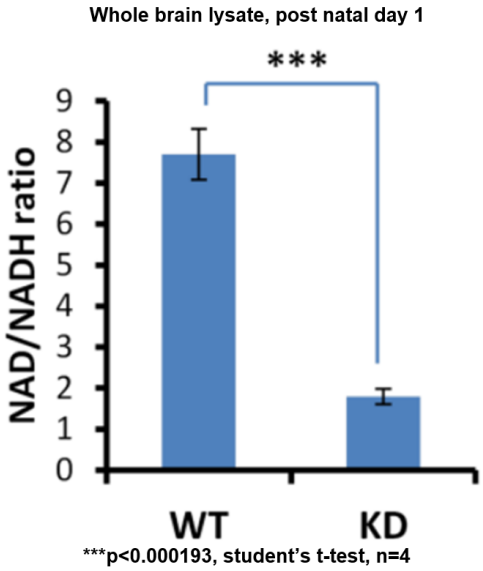

Figure 9. Reduction in NAD/NADH ratio in Nipsnap1 deficient mice. Lysates were prepared from post-natal day 1 cortex of Nipsnap1 (n=4) and WT (n=4) animals. NAD+ and NADH levels were measured enzymatically using spectrophotometric assay EnzyChromTM NAD+/NADH assay kit (E2ND-100, BioAssay Systems, CA) according to manufacturer's protocol. We found that Nipsnap1 deficiency resulted in lower NAD+ and higher NADH concentrations in the brain. Importantly, the NAD/NADH ratio was significantly ($p<0.000193$, student's t-test, n=4) lower in Nipsnap1 KD brains (Qiao unpublished).

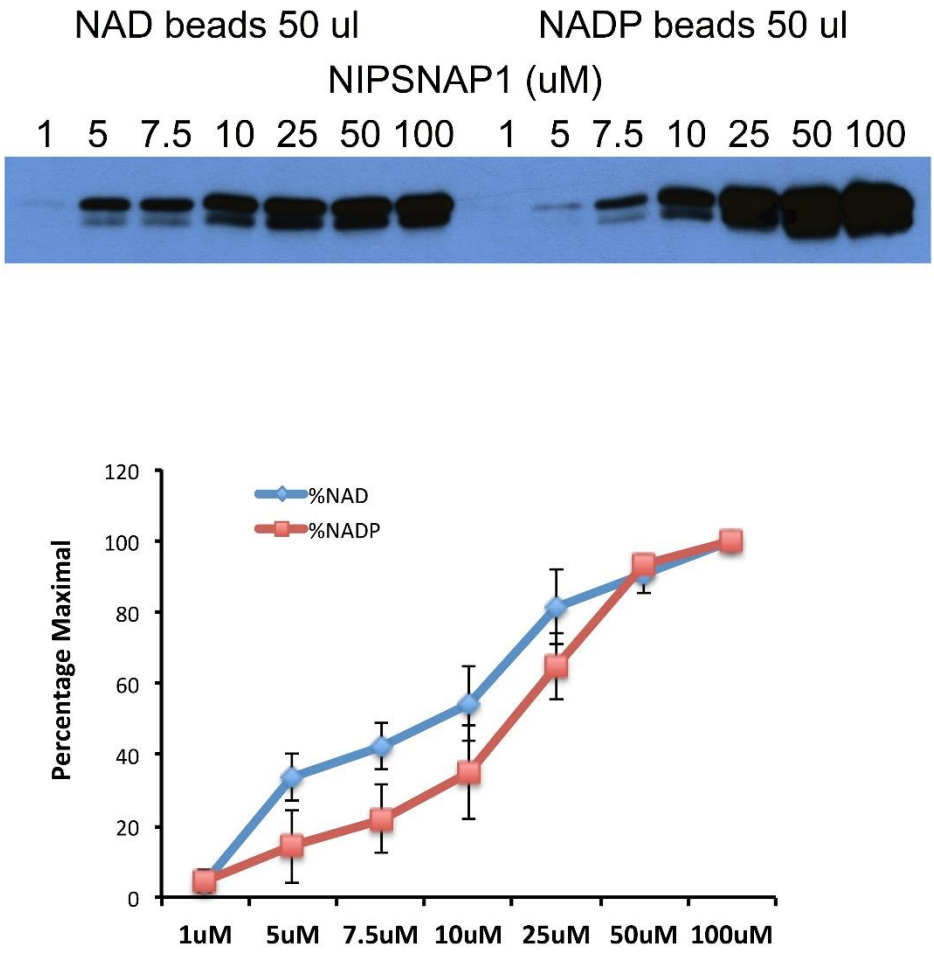

Figure 10. Biochemical pull-down using NAD(P). Experiments displayed direct binding of purified recombinant Nipsnap1 protein to NAD+ and NADP+ immobilized sepharose beads (Qiao unpublished).

To test if Nipsnap1 binds to NAD+ and NADP+ directly, it is necessary to generate large amounts of recombinant Nipsnap1 protein. Previous work focused on expressing His-Tagged recombinant protein using a pET-28a plasmid containing an *E. coli* optimized form of the mouse Nipsnap1 gene, minus the mitochondrial targeting

sequence (Gacasan unpublished). This expression system was used to perform preliminary biochemical binding assays, where purified recombinant Nipsnap1 was incubated with NAD+ or NADP+ immobilized on sepharose beads. Nipsnap1 was shown to bind to both NAD+ and NADP+ in a concentration dependent manner (Figure 10), with a slightly higher affinity for NAD+ than NADP+. The Nipsnap1-NAD+ interaction was further confirmed using circular dichroism (CD) spectroscopy (see results section, Figure 17), indicating Nipsnap1 undergoes a structural change in the presence of NAD+.

Project Goals

To carefully analyze the NAD binding characteristics of Nipsnap1, larger quantities of purified recombinant Nipsnap1 were required. In this study, several approaches and experimental conditions were tested to optimize Nipsnap1 yield. The pET-28a expression system had failed to give desired levels of Nipsnap1 protein after optimization of the protocol. With the aim of increasing expression, three new Nipsnap1 constructs were developed based on the glutathione S-transferase (GST) fusion protein strategy. The expression, solubilization, and purification methods using the above constructs were then optimized in attempts to maximize the yield of soluble protein for additional biochemical characterization.

II – METHODS

Initial expression, purification, and analysis of Nipsnap1 using pET-28a system

Expression of Nipsnap1-pET-28a Construct

Escherichia coli BL21 (DE3) cells (EMD Millipore) were transformed using pET-28a plasmid containing Nipsnap1. Cells were grown in Luria-Bertani (LB) media containing kanamycin (30 mg/mL; Acros) at 37°C, with vigorous shaking. Nipsnap1 gene expression was induced using 0.1 mM isopropyl β-D-1-thiogalactopyranoside (IPTG) (Fisher) once an OD_{600} = 0.6 was reached, and cultures were grown for 6 hours post-induction, again at 37°C. Cells were harvested by centrifugation (Sorvall RC-5B Refrigerated Superspeed Centrifuge) at 6,000xg for 10 min at 4°C, and the resultant pellets stored at -80°C.

Cell lysis

Cell pellets (1 L) were resuspended in 40 mL buffer A (20 mM $NaPO_4$, 0.5 M NaCl. and 40 mM imidazole, pH 7.4; Fisher Scientific) containing lysozyme (0.2 mg/mL), benzonase nuclease (1000 units) and a protease-inhibitor cocktail, all from Sigma-Aldrich. The cell suspension was sonicated, on ice, at 50% power with pulsing for 5 min using a Biologics, Inc. Ultra Sonic Homogenizer Model 150 VT, then placed on a rocker for 30 min at room temperature. The resultant lysate was centrifuged at 8,000xg for 20 min using an AccuSpin 4000 table-top centrifuge. The supernatant, the soluble cellular fraction, was collected and sterile-filtered using a 0.22 μM filter (EMD Millipore).

Purification of Nipsnap1-His recombinant protein

The His-tagged Nipsnap1 protein was purified using Ni-Affinity chromatography. Supernatant was cycled onto a 1 mL Ni sepharose HisTrap HP column (GE Health Sciences) for 1-2 hours at 4°C, using a peristaltic pump, to ensure maximum protein binding. The column was then washed with buffer A for 20 min, to remove any nonspecifically bound protein, and the bound protein eluted with buffer B (20mM Na_3PO_4, 0.5M NaCl, and 500mM imidazole, pH 7.4). Purity was evaluated using Coomassie staining and Nipsnap1 presence was validated by immunoblot analysis (Figures A1 and A2).

Circular dichroism spectroscopy

Purified His-tagged Nipsnap1 was analyzed via circular dichroism (CD) spectroscopy, using an AVIV Circular Dichroism Spectrometer Model 410SF. For initial runs, 750 uL 7.39 uM Nipsnap1 was diluted with 250 uL 1XTBS (50 mM Tris, 150 mM NaCl, pH 7.6) and near-UV wavelengths (350-250 nm) were scanned. Additional near-UV scans were performed using 750 uL 1XTBS mixed with 250 uL 0.02 M NAD+, and 750 uL 7.39 uM Nipsnap1 mixed with 250 uL 0.02 M NAD+.

Nipsnap1 expression and optimization using pGEX-4T1 vector

An overview of the expression system and purification strategy is shown in Figure 11 and explained in detail in sections below.

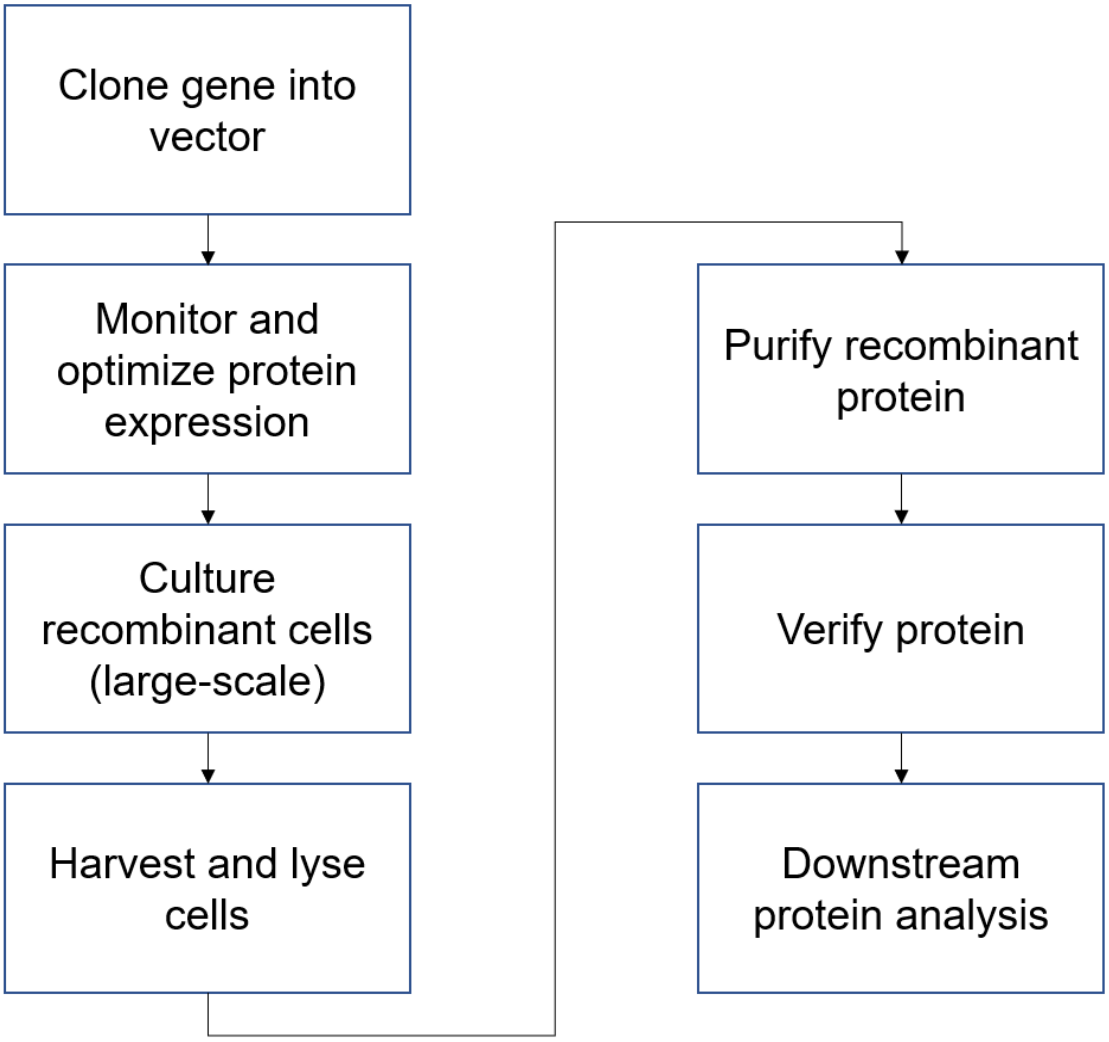

Figure 11. Diagram showing approach to developing a recombinant Nipsnap1 purification system using the pGEX plasmid. The Nipsnap1 gene was cloned into pGEX4T-1, its protein expression optimized, and large-scale cultures generated. Cells were lysed via sonication, and supernatants, were used in protein purification. Protein verification was performed using Coomassie staining and immunoblot analysis.

Nipsnap1-pGEX-4T1 expression construct

Mouse Nipsnap1 coding sequence (NCBI Gene ID: 18082) was cloned in-frame to GST using the pGEX-4T1 plasmid (Sigma). A plasmid map of the pGEX-4T1 plasmid is shown in Figure 12. The pGEX-4T bacterial expression vector (GE Healthcare Life Sciences) contains the GST gene in its multiple cloning site. The wild type mouse Nipsnap1 gene minus the mitochondrial signal sequence was sub-cloned into pGEX-4T-1 using the EcoRI and NotI restriction sites found in the plasmid multiple cloning site. Custom oligonucleotides were purchased from Integrated DNA Technologies. Primers shown in table 2 were used to introduce the respective restriction sites to the ends of the wild type Nipsnap1 gene by PCR using Q5 High-Fidelity DNA polymerase (New England Biolabs).

Table 2. Primers used to introduce Nipsnap1 into pGEX-4T1. Red, blue, and green nucleotides correspond to start/stop codons, restriction sites, and additional nucleotides to bring primer GC content and melting temperature (Tm), respectively, into more optimal ranges for use in PCR.

Mouse cDNA Primers	Sequence	GC %	Predicted Tm (C)
Forward (EcoRI)	ATACAGAATTCATGGGGGACCTCGCGGCTGC	58.06	67.7
Reverse (NotI)	GTGAGGCGGCCGCTCACTGGAGAGGAGAAATC	62.5	68.6
C-Terminal Truncation Fwd (EcoRI)	GCGCAGAATTCATGGCCCTCATGGACTGCATG	56.25	67
N-Terminal Truncation Rev (NotI)	GTGAGGCGGCCGCTTACCTGGACAGCAGCATCTTGC	63.89	71.7

Three plasmids were designed, each resulting in a different final form of the protein, (Full length: Nipsnap1-FL, N-terminal fragment: Nipsnap1-NTF, C-terminal fragment: Nipsnap1-CTF, see Figure 13). This was done to localize any interactions Nipsnap1 has to specific parts of the protein. Due to the high evolutionary conservation of the NIPSNAP protein family C-terminus, we hypothesized any conserved functions would be localized to this region.

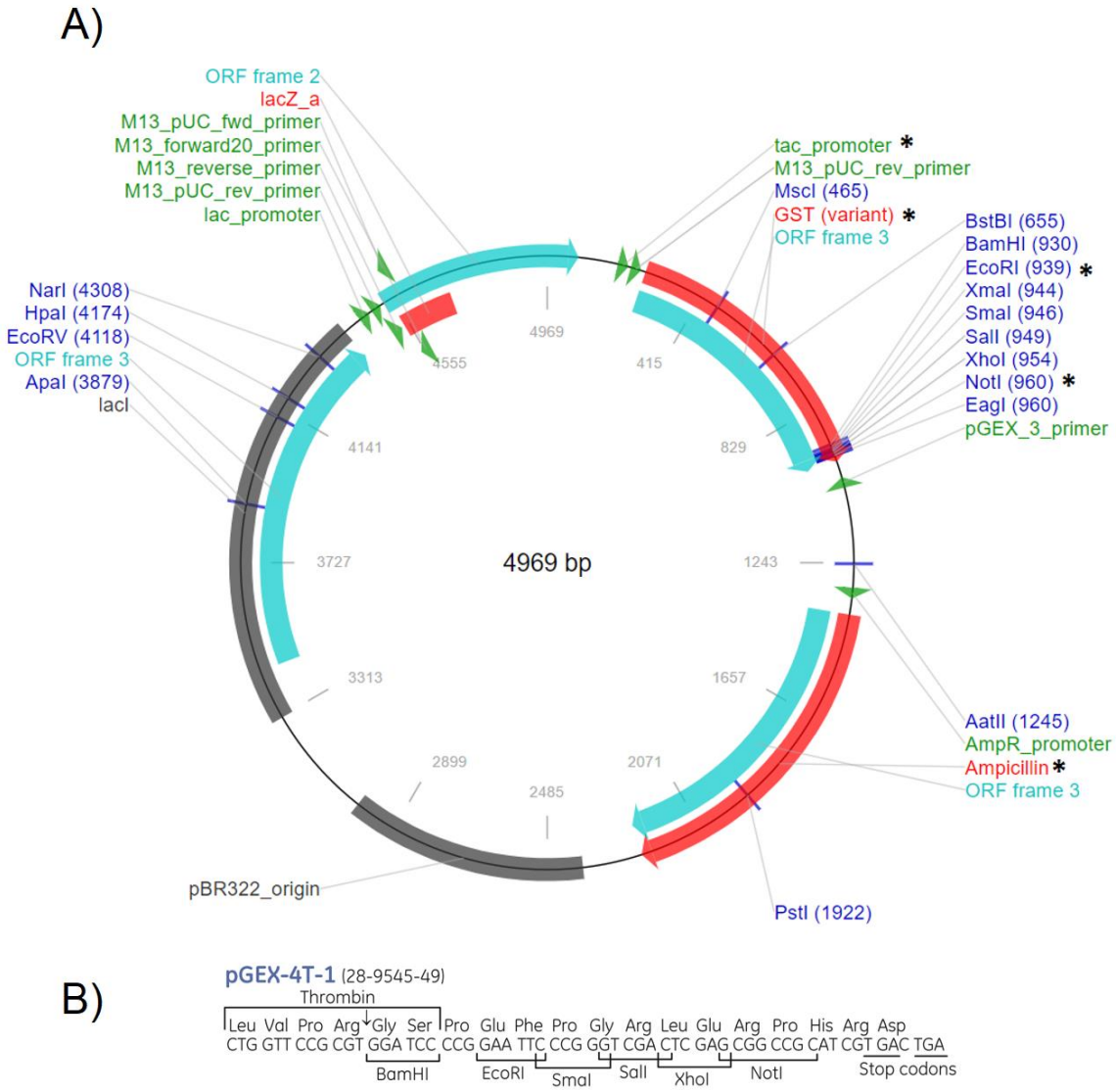

Figure 12. A) Plasmid map of the pGEX-4T1 plasmid (addgene). Relevant functional sites utilized in our expression system are denoted by an *. Nipsnap1 was introduced into the GST variant site controlled by the tac_promoter using the forward primer EcoRI High-Fidelity (HF) (NEB) and reverse primer NotI HF (NEB) using Platinum Taq DNA Polymerase (Invitrogen) and T4 DNA Ligase (NEB). B) Primary sequence displaying the thrombin cleavage and restriction sites.

Our lab previously generated a Nipsnap1 antibody that recognizes the epitope NKLKNNKEYLEFRKER; Nipsnap1 constructs were designed keeping this region of the protein in mind (Figure 13). Due to the epitope being localized in roughly the middle of the protein, we adjusted the sizes of each truncated construct relative to their original pET-28a forms to allow for more convenient and precise immunoblot analysis. The nucleotide sizes and predicted molecular weight of the expressed protein for each of the Nipsnap1 forms are found in Table 3.

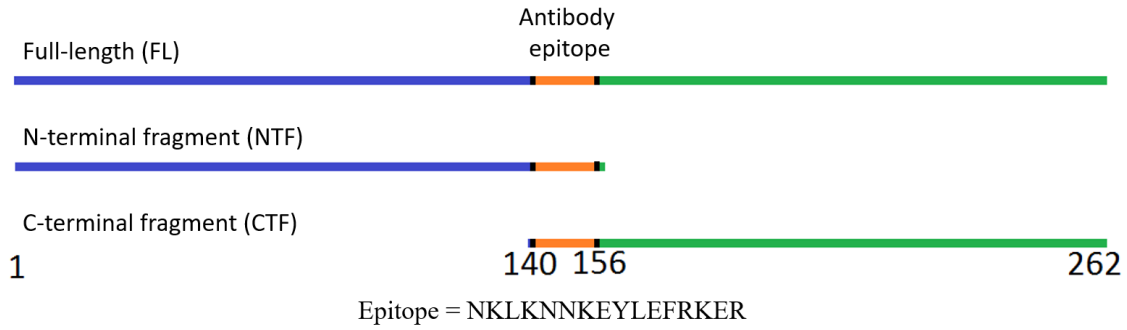

Figure 13. Design map for the three Nipsnap1 constructs developed. FL Nipsnap1 has a predicted AA length of 262 residues. Our generated antibody recognizes the epitope shown corresponding to AA140-156. The N-terminus of the protein has been defined as AA 1-140 shown in blue, with the NTF protein including the entire N-terminus, epitope, and a slight portion of the C-terminus. The C-terminus is shown in green, with the CTF protein including the entire C-terminus, epitope, and a slight portion of the N-terminus. Slight hangover of the other termini is purposely designed in order to ensure epitope recognition.

Table 3. Summary of predicted sizes for Nipsnap1 cDNA and protein. Initial protein exists as a GST-Nipsnap1 fusion protein. Nipsnap1 is cleaved from the 27 kDa GST during purification.

Form	Expected cDNA size (bp)	Fusion protein size (kDa)	Cleaved protein size (kDa)
FL Nipsnap1	813	57	30
NTF Nipsnap1	447	43	16
CTF Nipsnap1	483	45	18

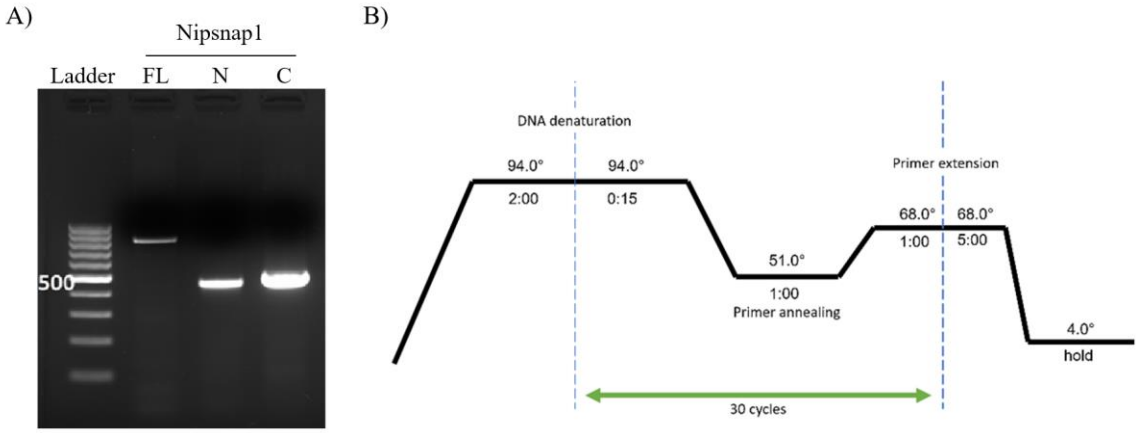

Figure 14. A) Nipsnap1 cDNAs generated via PCR amplification. All three cDNAs appear at the correct approximate size. B) Diagram of amplification strategy.

Both the pGEX-4T1 plasmid (not shown) and Nipsnap1 cDNA (Figure 14) were digested using EcoRI and NotI restriction enzymes, ligated together, and the ligation products used to transform E. coli DH5α cells (Invitrogen). DNA sequences for all three constructs were verified through the Molecular Resource Center, University of Tennessee Health Science Center, Memphis, TN.

Bacterial culture and growth curve preparation

The verified Nipsnap1-FL pGEX-4T-1 plasmid or empty vector control was used to transform *E. coli* BL21(DE3)pLysS Competent Cells (Promega). Cells were grown in Luria-Bertani (LB) media containing ampicillin at 37°C, with vigorous shaking. Once an OD600=0.6 was reached, cultures were split into four 10 mL cultures and supplemented with 0.1 mM IPTG and/or NAD+ as shown in Figure 15. OD readings were measured hourly for six hours for all four conditions.

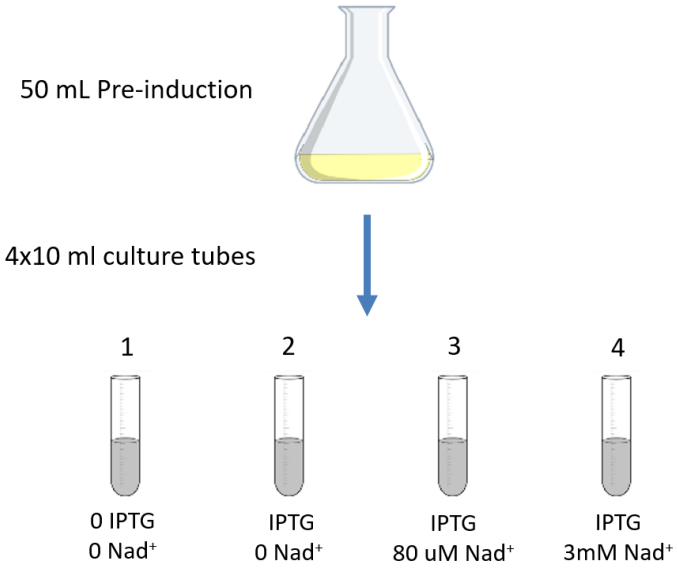

Figure 15. Schematic of bacterial growth curve experimentation. BL21(DE3)pLysS Competent Cells were transformed with either FL Nipsnap1 pGEX-4T1 or empty pGEX-4T1 control. Ten mL overnight culture was diluted to 50 mL and grown until OD600 = 0.6, and then separated into four 10 mL fractions. Fractions were either supplemented with NAD+ and/or IPTG (0.1 mM) or nothing, as shown in the conditions numbered above.

Initial pGEX-4T1 Nipsnap1 expression and purification

Nipsnap1 expression using pGEX-4T system

The verified Nipsnap1 pGEX-4T-1 plasmids were used to transform E. coli BL21 (DE3) cells (EMD Millipore). Cells were grown in LB media containing 50 ug/mL ampicillin at 37°C, with vigorous shaking. Nipsnap1 gene expression was induced using 0.1 mM IPTG (Fisher) once an OD600=0.6 was reached, and cultures grown for 6 hours post-induction, again at 37°C. Cells were harvested by centrifugation (Sorvall RC-5B Refrigerated Superspeed Centrifuge) at 6,000xg for 10min at 4°C, and the resultant pellets stored at -80°C.

Bacterial lysis

The cell pellet was resuspended in binding buffer (PBS: 140 mM NaCl, 2.7 mM KCl, 10 mM Na_2HPO_4, 1.8 mM KH_2PO_4, pH 7.4) containing benzonase nuclease (1000 units) and protease-inhibitor cocktail. The cell suspension was sonicated, on ice, at 50% power with pulsing for 5 min using Biologics, Inc. Ultra Sonic Homogenizer Model 150 VT. The resultant lysate was centrifuged at 16,000xg for 90 minutes at 4°C. The supernatant, the soluble cellular fraction, was collected and sterile-filtered using a 0.22 μM filter (EMD Millipore).

Table 4. Buffers used in GST-based protein purification.

Buffer A1 (PBS)	
pH	7.4
Reagent	**Concentration**
NaCl	140 mM
KCl	2.7 mM
Na_2HPO_4	10 mM
KH_2PO_4	1.8 mM

Buffer A2	
pH	8
Reagent	**Concentration**
Tris	50 mM
Glutathione (red.)	20 mM

Buffer B1	
pH	7.5
Reagent	**Concentration**
Na_3PO_4	20 mM
NaCl	1.0 M

Buffer B2	
Reagent	**Concentration**
p-aminobenzamidine	20 mM
NaCl	140 mM
KCl	2.7 mM
Na_2HPO_4	10 mM
KH_2PO_4	1.8 mM

A glutathione-s-transferase (GST) fusion system was utilized for affinity purification (GE Healthcare Life Sciences). Buffers used during purification are detailed in Table 4, and a complete workflow of the purification strategy is shown in Figure 16. Purification of GST-bound Nipsnap1 was performed using GSTrap FF and HighTrapBenzamidine columns from GE Healthcare Life Sciences. Clarified lysate from bacteria expressing GST-fused Nipsnap1 was cycled onto the GSTrap FF column for 90 min at 4°C. The GSTrap FF was washed with 5 volumes PBS, then 1 mL of PBS containing 1 U/ul thrombin was introduced into the column, then incubated for 4 h at room temperature. The GSTrap FF column was then connected to a HiTrap Benzamidine FF column, and Nipsnap1 was eluted from the column using buffer B1. Columns were disconnected, GST was washed from the GSTrap FF column with buffer A2, and thrombin off the HiTrap column using buffer B2.

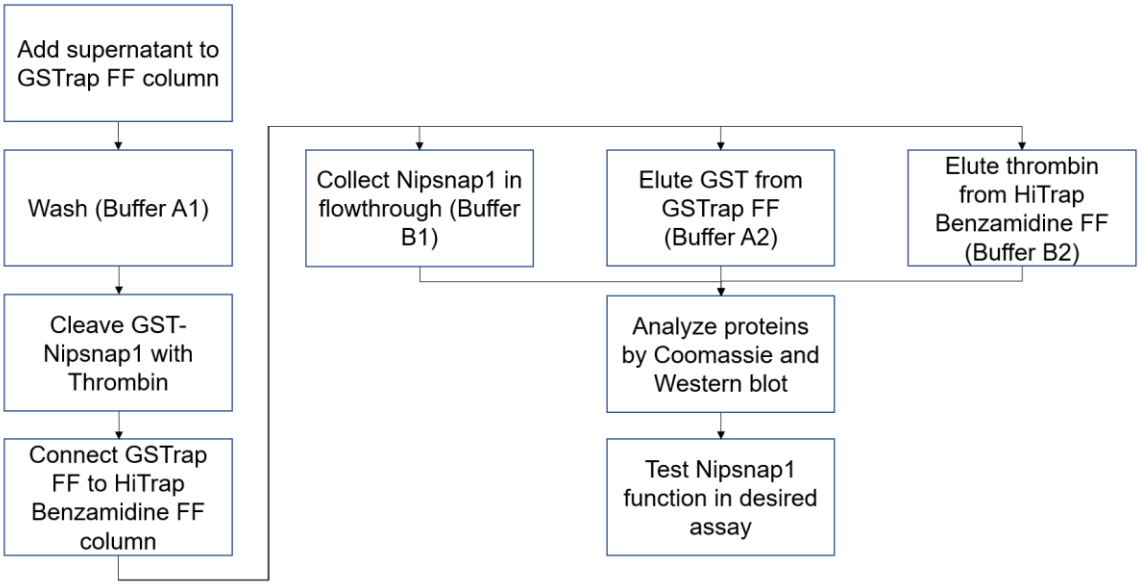

Figure 16. Workflow of GST purification strategy (GE Healthcare Life Sciences). Lysate is loaded on-column and washed with 5 column volumes PBS to remove nonspecifically bound proteins. Thrombin suspended in PBS is loaded on-column and allowed to incubate at room temperature to cleave the fusion protein from bound GST. Following incubation, the GSTrap FF is connected to a HiTrap benzamidine column. Buffer B1 is eluted through the columns, resulting in thrombin removal from the sample by binding the HiTrap Benzamidine FF column, and elution of cleaved Nipsnap1 out of the columns.

Sample purification was validated by Coomassie staining to visualize protein purity and estimate which fractions contained Nipsnap1 after purification. Western blot analysis was subsequently performed to verify Nipsnap1 presence in eluted fractions (Figure 19).

Optimization of Nipsnap1 induction

Nipsnap1 induction was optimized by altering several conditions and observing which gave the highest levels of induced Nipsnap1 protein. Conditions altered include post-induction incubation time, temperatures used in post-induction incubations, media composition, and IPTG concentrations given for protein induction.

Post-induction time at 37 °C

Cultures (10 mL, LB media) transformed with pGEX-4T1 control or Nipsnap1 (Nipsnap1-FL, Nipsnap1-NTF, or Nipsnap1-CTF) were incubated overnight at 37 °C. Cultures were diluted to 50 mL the following day and grown to an OD_{600} of 0.6 and induced using 0.1 mM IPTG. Aliquots (1 mL) were taken immediately before induction and 3 or 6 h after induction. Coomassie staining was used to visualize total protein for all constructs (Figure 20).

Post-induction time at 18 °C

Bacterial culture temperature post-induction was lowered in order to reduce the likelihood of shuttling of expressed protein into inclusion bodies (Figure 21). Cultures (10 mL, LB media) transformed with pGEX-4T1 control or Nipsnap1-NTF were incubated overnight at 30 °C. Cultures were diluted to 50 mL the following day and grown to an OD_{600} of 0.6 and induced using either 0.1 mM, 0.01 mM, or 0.001 mM IPTG. Post-induction, the temperature was then dropped from 37 °C to 18 °C, and growth was monitored at 6, 12, and 18 h to choose a suitable endpoint if there were noticeable differences in protein expression (Figure 21).

Comparison of post-induction temperatures

To determine if the 18 °C induction-based protocol gives better Nipsnap1 yield than the original 37 °C induction-based protocol, lysates and supernatants were generated according to both protocols (Table 5) and evaluated after sonication using the new sonication conditions. Protein yield was determined by Coomassie (Figure 22) staining and Western blot analysis (Figure 23).

Table 5. Summary of conditions used in comparison of 18 °C and 37 °C induction.

Nipsnap1 induction	37°C	18°C
O/N temperature (°C)	37	30
Preinduction temperature(°C)	37	37
Post-induction temperature (°C)	37	18
Induction times (hr)	3	6
IPTG concentration (mM)	0.1	0.075

IPTG concentration effects

Cultures (10 mL, LB media) transformed with pGEX-4T1 control or Nipsnap1-NTF were incubated overnight at 30 °C. Cultures were diluted to 50 mL the following day and grown to an OD_{600} of 0.6 and induced using either 0.1 mM, 0.01 mM, or 0.001 mM IPTG. Cultures were incubated at 18 °C, and growth monitored at 6, 12, and 18 h. Samples were lysed according to initial protocol (Table 5) and lysates and their resulting soluble fractions were visualized by Coomassie staining. (Figure 21)

Optimization of Nipsnap1 solubilization

Optimization of Nipsnap1 solubilization was achieved by altering sonication procedures and lysis conditions (NP40 or lysozyme).

NP40 and lysozyme mediated solubilization

Cultures (10 mL, LB media) transformed with pGEX-4T1 control or Nipsnap1-NTF were incubated overnight at 37 °C. Cultures were diluted to 50 mL the following day and grown to an OD_{600} of 0.6 and induced using 0.1 mM IPTG and incubated for 3 h. Bacteria were pelleted at 8000 RPM for 20 min, and resuspended in either PBS, PBS

supplemented with 1% NP40, lysozyme, or both. Samples were incubated on ice for 20 min, then lysed via an initial sonication method (Table 6) and 1 mL aliquots of lysate taken. Cell lysates were cleared, and soluble fractions collected as described above. The resulting pellets were resuspended in PBS/1% NP-40 and sonicated again for 3 minutes, aliquots of the suspension collected, then again centrifuged and supernatant collected. Coomassie staining was used to visualize all collected samples (Figure 25).

Optimization of sonication procedure

Overnight bacterial stocks (10 mL) containing empty pET-28a, pET CTF-Nipsnap1, empty pGEX, or pGEX CTF-Nipsnap1 were incubated overnight at 30 °C. Samples were diluted to 50 mL LB/1% glucose, and grown at 37 °C until OD600 = 0.6, then induced with IPTG and allowed to incubate at 18 °C for 6 h. Bacteria were pelleted at 8000 RPM for 20 min, and then lysed using a new sonication protocol (20% power, 1:1 on/off 50% pulsing, x3 cycles; wait 5 min, repeat cycle 2x – a total of 3 x 30 sec cycles). Samples were visualized by Coomassie staining (not shown) and Western blot analysis (Figure 24). A comparison of the initial and final sample protocols is shown in table 6.

Table 6. Comparison of initial and final solubilization protocols.

Sonication procedure	Initial	Final
Power (%)	50	20
Pulsing	50	50
Duration (min)	5	0.5
Rest time (min)	5	5
Number of cycles	2	3

Optimization of Nipsnap1 elution

Optimization of Nipsnap1 purification was achieved by increasing thrombin incubation time to facilitate an increase in Nipsnap1 cleavage from GST. A 50 mL bacterial culture (CTF-Nipsnap1, empty GST) was centrifuged at 14,000 RPM for 20 min. Resulting pellets were resuspended in 20 mL PBS/PIC and sonicated on ice for 5 min with pulsing at 50% power twice. The sample was centrifuged for 90 min max speed, and the supernatant loaded on GSTrap FF 1mL using a peristaltic pump for 1 hour at 1 mL/min. Five column volumes PBS were used in washing (W fraction). The thrombin solution (1 mL) was then loaded onto the GSTrap column and incubated for 25 hours. Five column volumes PBS were used to elute the cleaved Nipsnap1 (Cleavage, C fraction), then five column volumes buffer A2 were used to elute GST (elution fraction, E).

A sample of the fractions were evaluated by Coomassie staining (Figure 28). Thrombin incubation duration was also evaluated at additional timepoints (18 and 20 h) and for Nipsnap1-NTF (not shown).

Large-scale Nipsnap1 expression and purification

The verified Nipsnap1 pGEX-4T-1 plasmids were used to transform *E. coli* BL21 (DE3) cells (EMD Millipore). Cells were grown in LB media containing ampicillin at 37°C, with vigorous shaking. Nipsnap1 gene expression was induced using 0.1 mM IPTG (Fisher) once an OD600=0.6 was reached, and cultures were spun down 3 h post-induction, and the resulting pellet was suspended in 80 mL PBS. Sonication (20%pwr, 1s on/off, sit on ice 5 min, 3X) was performed and resulting lysate centrifuged for 1 h at 20,000xg/4°C. Supernatant was loaded onto the GSTrap FF column for 90 minutes, washed with five column volumes of PBS, and then incubated with thrombin for 25 h at room temperature. The GSTrap FF column was connected to the HiTrap benzamidine FF column, and five column volumes buffer B1 used to elute cleaved protein. GST and thrombin were eluted from their respective columns using buffers A2 and B2, respectively. Coomassie staining (Figure 29) and Western blot analysis (Figure 30) were used to verify Nipsnap1 purification and compare total protein yield with bacteria transformed with control pGEX-4T1.

III – RESULTS

CD spectroscopy indicates interaction with NAD+ causes a structural shift in Nipsnap1

CD spectroscopy is a valuable technique for the analysis of protein features in solution and can be used to observe conformational changes of a protein in the presence of ligand (Kelly 2005). Near-UV CD data derived from Nipsnap1-FL purified in the pET-28a purification system and NAD+ is shown in Figure 17. Marked changes in the Nipsnap1 near-UV spectrum appear in the presence of NAD+ (i.e., development of the large peak at 300 nm in the Nipsnap1-NAD+ spectrum), suggesting a shift in Nipsnap1 tertiary structure. Subtraction of the Nipsnap1 and NAD+ spectra from the Nipsnap1-NAD+ spectra supports the hypothesis that NAD+ binding produces a structural change in Nipsnap1 and is in agreement with previously derived data generated in biochemical pulldowns of Nipsnap1 using NAD+ linked sepharose beads.

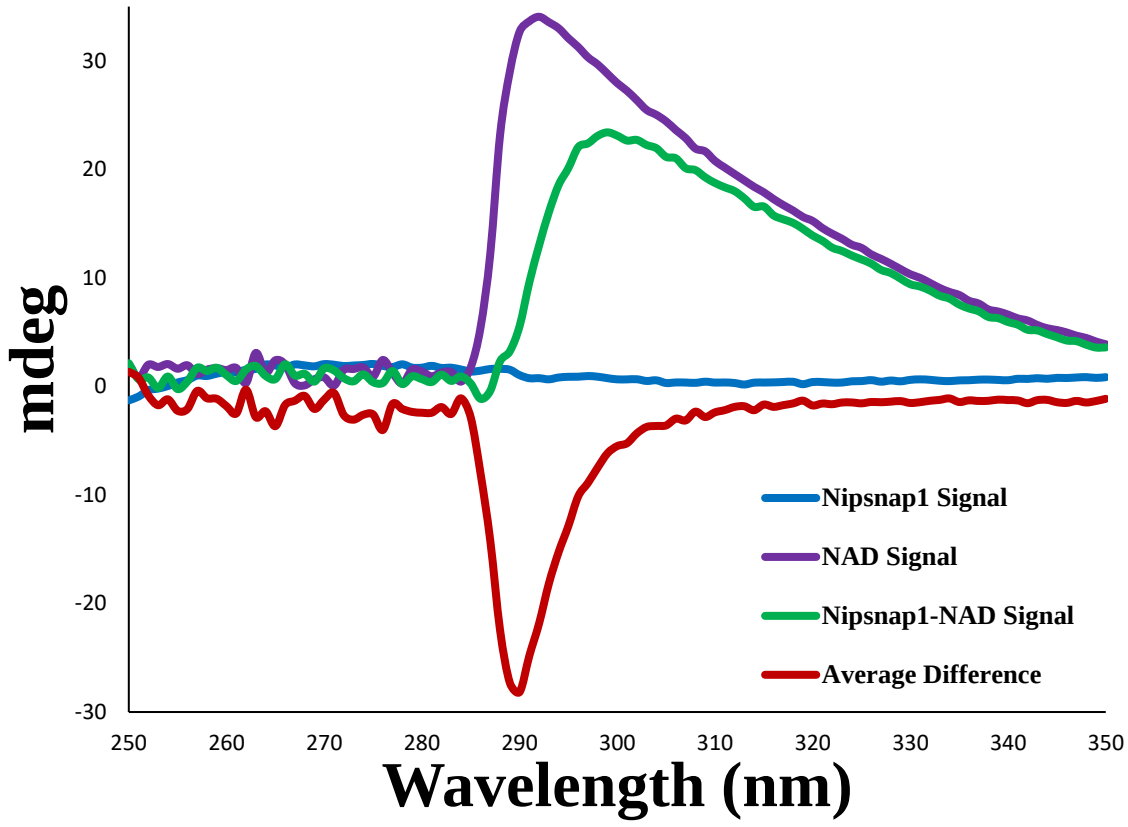

Figure 17. Circular dichroism spectra for Nipsnap1, NAD+, and Nipsnap1 mixed with NAD+. A difference spectrum was generated by subtracting the Nipsnap1 and NAD+ spectra from the Nipsnap1-NAD+ spectrum in the near-UV, indicating Nipsnap1 undergoes a structural change in the presence of NAD+.

Nipsnap1 expression does not affect growth of BL21(DE3)pLysS Cells

The observation that Nipsnap1 binds NAD+ suggests that Nipsnap1 may affect NAD+ utilization and metabolism, thereby compromising bacterial growth. We hypothesized that Nipsnap1 expression in *E. coli* results in a bacteriostatic effect, and that NAD+ supplementation may improve bacterial growth. We tested this by generating bacterial growth curves using the scheme in Figure 15. Both a physiologically relevant and high concentration of NAD+ as reported previously were used in addition to unsupplemented medium (Yongjin 2011).

As shown in Figure 18A, bacterial growth was similar between cells transformed with pGEX-4T1 Nipsnap1 compared to empty vector control. IPTG-induced cells had a general reduction in growth rate. This is most likely attributed to induced cells having a higher metabolic burden from increased protein synthesis following induction. Additionally, the growth curves display a shift and plateau effect on log phase across all induced samples. Uninduced cells appear to have increased bacterial growth during log phase. Nipsnap1-expressing cells appeared to have slightly lower growth rates than vector control samples. However, this difference did not appear to be significant.

As displayed in Figure 18B, no significant differences in growth curves for non-induced BL21(DE3)pLysS Competent Cells were detected, allowing conclusions to be drawn if differences are observed between Nipsnap1 expressing cells and controls. However, NAD+ supplementation at physiological concentrations (80 uM NAD+) shows a significant difference in bacterial growth between Nipsnap1 inducing cells compared to control. This effect is diminished when NAD+ is supplemented at a physiologically extreme concentration (3 mM). The mechanism by which the differences in bacterial growth in the presence of NAD+ between Nipsnap1 expressing cells and control manifest is not known at this time.

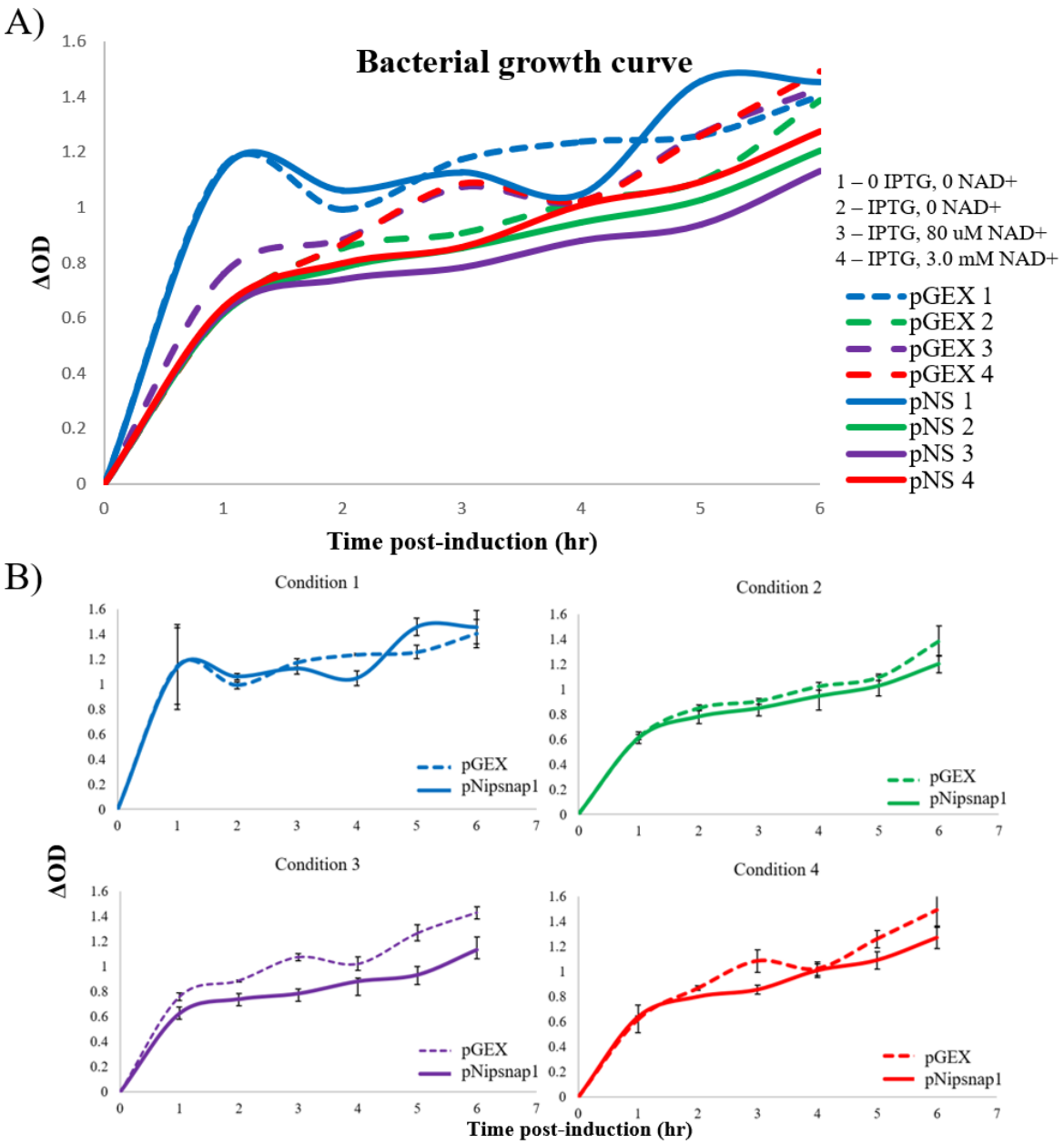

Figure 18. Bacterial growth curves generated pGEX-4T1 transformed cells (n=3). A) All growth curves overlaid. cells transformed using pGEX-4T1 encoding Nipsnap1 are shown in solid lines, and empty pGEX controls by dashed lines. pGEX denotes cells that were transformed using empty pGEX-4T1 plasmid, pNS denotes cells transformed with Nipsnap1; number next to the plasmid denotes condition. B) Nipsnap1-transformed cells versus control in each of the four conditions. Condition 1 was not induced and had no NAD+ supplementation, condition 2 was induced without supplementation. Conditions 3 and 4 are induced with low and high levels of NAD+ supplementation, respectively.

Initial parameters for Nipsnap1 induction and solubilization were not optimal

A Coomassie stain of SDS-PAGE separated bacterial proteins following an initial solubilization procedure is shown in Figure 18. Nipsnap1-NTF (expected size ~43 kDa) level was greatly reduced after centrifugation of the lysate to acquire the soluble fraction that is loaded on the affinity column. Eluted fractions are not shown due to a lack of protein. These results indicate that the vast majority of the induced Nipsnap1 protein remained in the insoluble fraction. Therefore, a step-wise strategy to optimize the expression, solubilization, and purification protocols to enhance protein yield was begun. Conditions tested included bacterial culture time, temperature, broth composition, and concentration of IPTG used in induction. Optimization of each of these conditions are described in detail in the following sections.

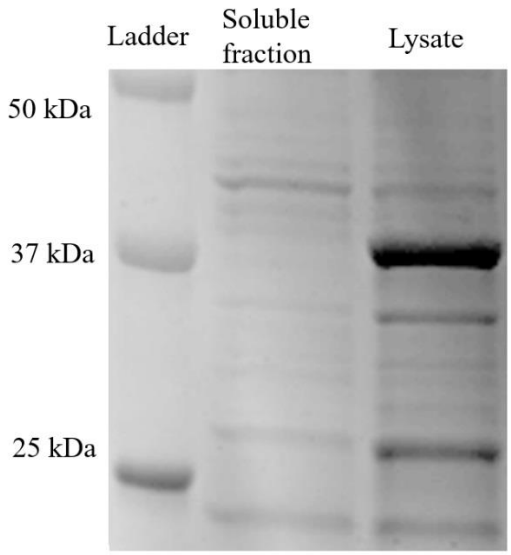

Figure 18. Coomassie stain showing initial attempt at purification. NTF Nipsnap1 was induced and grown at 37 °C for 6 h and lysed using initial method. Column was incubated with thrombin for 4 hours. Wash and elution fractions not shown due to showing no protein by Coomassie. NTF Nipsnap1 (43 kDa) protein is greatly reduced in soluble fraction compared to lysate.

Optimization of Nipsnap1 induction

Duration of incubation time has little effect on total protein

First, length of time for bacterial growth post-IPTG induction for all three Nipsnap1 constructs at 37°C (see Table 5 in methods) was compared to empty vector GST control (Figure 20). In general, induction of Nipnsap1 proteins were at comparable levels to GST control. Specifically, slightly lower induction was observed for Nipsnap1-FL (57 kDa), whereas higher levels were observed Nipsnap1-NTF and Nipsnap1-CTF as compared to GST control. In addition, 3h induction appeared to produce maximal protein expression. However, a slight reduction in Nipsnap1-CTF (~40 kDa) was seen between 6 h to 3 h incubation periods. No differences were seen in Nipsnap1-NTF samples. In conclusion, it appears that duration of incubation post-induction had little effect on total protein across all samples.

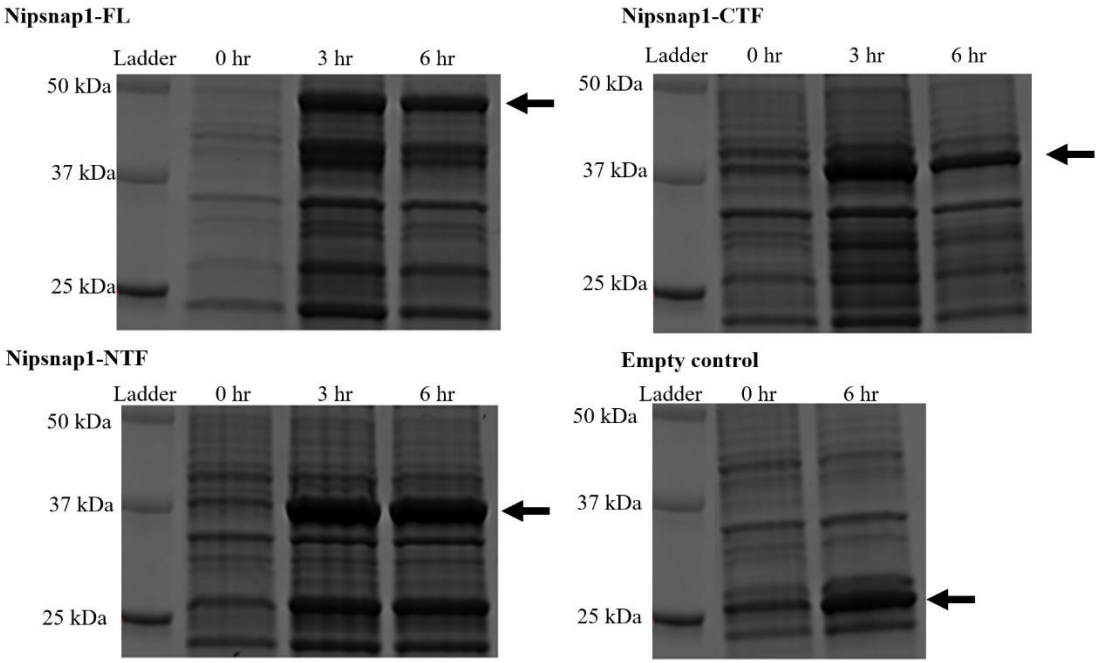

Figure 20. Coomassie stain of induced lysate samples and control. Ladder (L) is shown for molecular weight comparison purposes. Reduction in induced protein was observed between Nipsnap1-FL/CTF and control (+) samples. Induced bands are denoted with arrows.

Post-induction incubation at 37 °C increased Nipsnap1 expression compared to 18 °C

Bacterial culture temperature post-induction was dropped from 37 °C to 18 °C in an attempt to decrease the growth rate and reduce the chance that the expressed protein is shuttled into insoluble inclusion bodies (Figure 21). Samples were taken at 6, 12, and 18 h post induction. Longer incubation times post-induction resulted in subtle increases in Nipsnap1 expression, with less difference between 12-18 h time points compared to 6-12 h. Based on these results, 6 h post-induction time point was chosen for the subsequent experiments.

Manipulating IPTG concentration had little effect on total protein induction at 18 °C.

The use of IPTG to induce protein expression from plasmids can result in pronounced physiological stress to *E. coli* (Dvorak 2015). Alterations in the concentration of IPTG and the resulting effect on Nipsnap1-NTF induction was explored by Coomassie staining (Figure 21). Coomassie staining indicated differences in IPTG concentration had little effect on total protein production. Higher concentrations of IPTG resulted in subtle increases in Nipsnap1 production.

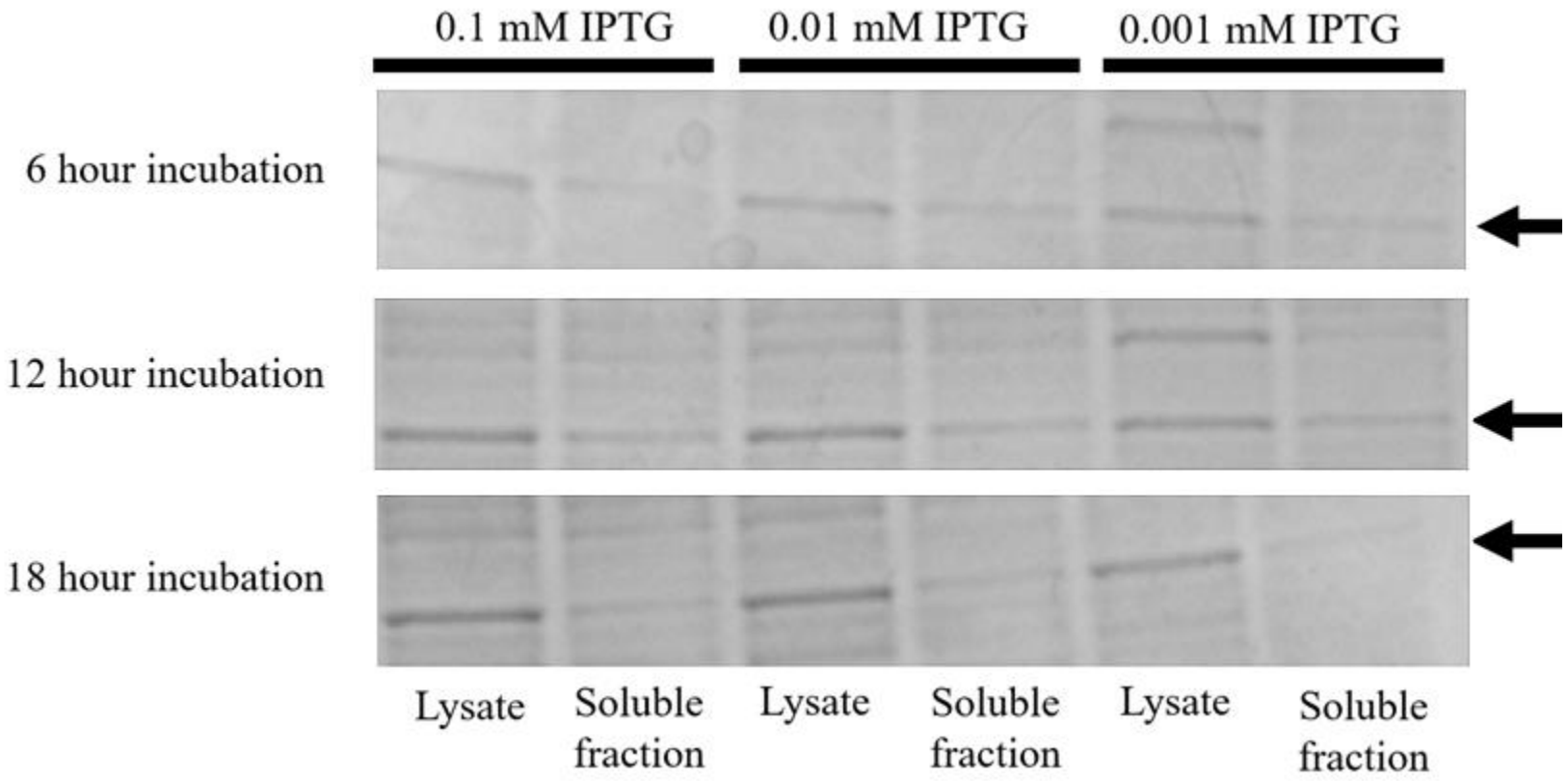

Figure 21. NTF Nipsnap1 expression in bacterial cultures induced with varying IPTG concentrations and grown for different times visualized by Coomassie. Concentrations of IPTG and induction times are noted, and induced Nipsnap1-NTF is denoted with arrow. Longer incubation times post-induction resulted in subtle increases in expressed Nipsnap1. The concentration of IPTG has little effect on total protein induction.

To determine if decreasing incubation temperature slows growth and increases production of soluble Nipsnap1 protein, bacterial lysates and supernatants were compared after induction at either 18 °C or 37 °C. Protein yield was determined by Coomassie staining (Figure 22). There were no noticeable differences in overall induction levels between the two protocols as detected by Coomassie staining, but Western blot analysis indicated the 37 °C-based protocol resulted in higher levels of Nipsnap1-CTF protein. Interestingly, the proportion of soluble Nipsnap1-CTF at the expected size (45 kDa) compared to the lysate was higher using the 18 °C induction procedure, although the overall level of induced protein in the lysate was lower than the 37 °C-based protocol. This result suggests that lowering the incubation temperature may allow more protein to be accessible for solubilization. An additional band can also be seen in immunoblot analysis between 50-75 kDa. This may be attributed to dimerization/cross-linking of Nipsnap1-CTF and a potentially truncated form of Nipsnap1. Alternatively, this may be due to a post-translational modification of the Nipsnap1-CTF protein.

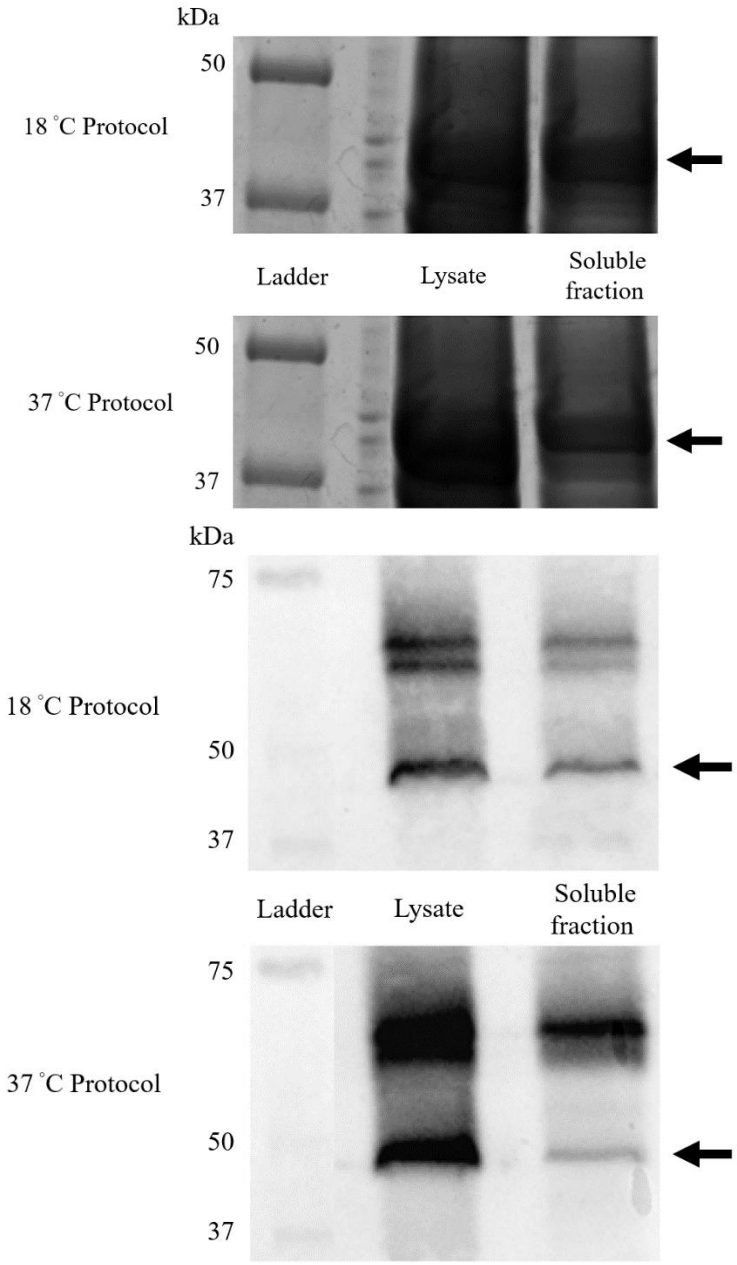

Figure 22. Temperature effect on protein expression. CTF Nipsnap1 was visualized by Coomassie staining (top two panels) or Western blot analysis (bottom two panels), comparing protein yields after sonication between 37 °C protocol 18 °C protocol or 37 °C protocol.

Optimization of Nipsnap1 solubilization

Lysozyme and NP40 addition did not increase the yield of soluble Nipsnap1

To increase the amount of protein in the soluble fraction, the addition of non-ionic detergent NP40 and/or lysozyme, a hydrolase that can compromise bacterial cell wall integrity, was examined for impact on Nipsnap1 recovery from the soluble fraction (Figure 23). Overall, no difference was observed in total soluble protein between the three conditions.

The strain of *E. coli* used in this study (BL21(DE3)pLysS) has been genetically engineered to express lysozyme, in order to help degrade cells walls after lysis has been initiated. Therefore, it was expected that supplementation of additional lysozyme would have no additional effect. NP40 is a non-ionic detergent often used to lyse membranes. Addition of NP40 may not be useful simply due to the harsh nature of sonication. In addition, NP40 does not seem to solubilize proteins that may be located in inclusion bodies.

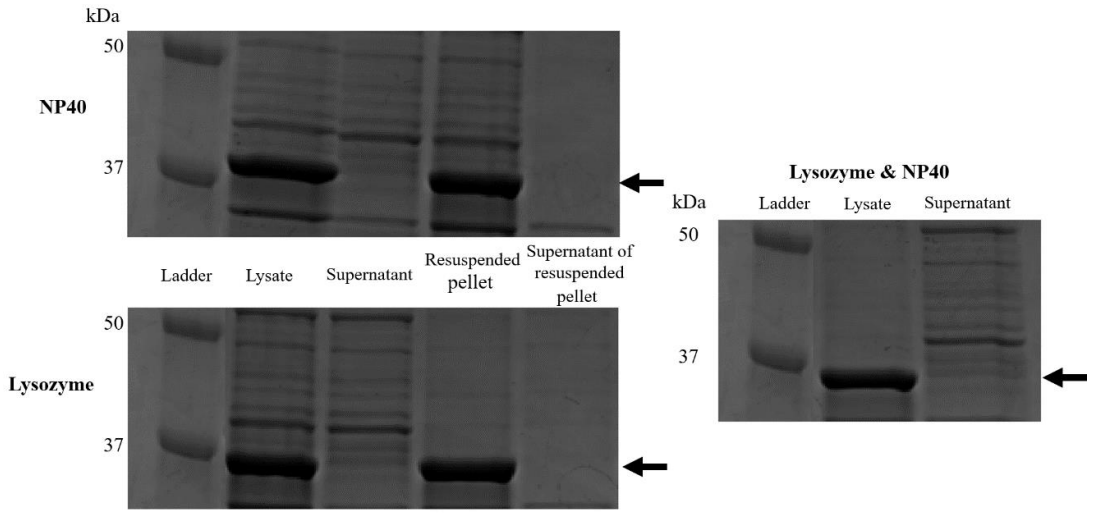

Figure 23. Coomassie stain comparing solubilization procedures using lysozyme or NP40. Pellets generated during lysate centrifugation were resuspended in either PBS with 1% NP40, lysozyme, or both. Generated solutions of PBS and pellet were incubated and again sonicated, aliquots were taken for analysis, then samples were again centrifuged, with the supernatants saved to be visualized by Coomassie. This was performed for all three conditions (NP40 addition, lysozyme addition, and addition of both).

Less stringent sonication conditions increased yield of soluble protein

Evidence suggests that prolonged sonication of bacterial cells may cause protein aggregation and fragmentation, resulting in the localization of expressed protein into ‘”apparent” inclusion bodies (Stathopulos 2004; Williams 1982). To address this issue, a less stringent sonication protocol was compared to the initial procedure (Table 6 in Methods), and samples were visualized by Western blot analysis (Figure 24). Western blot analysis demonstrates that a greater proportion of expressed Nipsnap1 was found in the soluble fraction using the milder sonication method in comparison to the proportion found in the soluble fraction using the initial sonication method. Western blot analysis also indicated that two forms of Nipsnap1 are being expressed, a faint band just above 37 kDa (expected size for Nipsnap1-CTF is 45 kDa) and an intense band just above 25 kDa.

The band at the desired size shows a reduction in Nipsnap1 intensity after collection of the soluble fraction. It is important to note that the pET-28a CTF Nipsnap1 does not contain the entire epitope sequence recognized by the used αNS1 antibody, and therefore cannot be visualized.

The predominant band at ~25 kDa is likely to be a truncated form of GST-Nipsnap1 that corresponds to the entire GST protein (26 kDa) and the initial segment of Nipsnap1-CTF containing the epitope sequence. This lack of complete protein translation could be the result of non-optimized codon usage in the plasmid, which encodes the mouse Nipsnap1 cDNA.

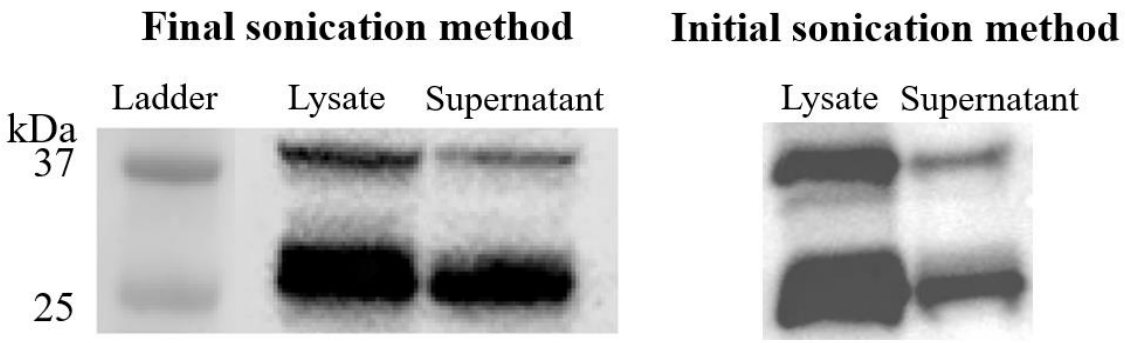

Figure 24. Comparison of Nipsnap1-CTF solubilization using initial and final sonication methods. A greater proportion of expressed Nipsnap1 is found in the soluble fraction for the milder sonication method in comparison to the proportion found in the soluble fraction using the initial sonication method. Initial and final Western blots were run separately.

Large-scale expression with optimized lysis and purification results in truncated Nipsnap1 proteins

To increase total protein yield, cultures transformed with pGEX4T1 containing Nipsnap1-CTF were scaled up to 1-liter and grown using the 37 °C based induction protocol and the modified sonication procedure (see methods). Protein levels were determined by Coomassie staining (Figure 25) and Western blot analysis (Figure 26). In general, much lower levels of Nipsnap1-CTF protein were induced than GST control when visualized by Coomassie staining (Figure 25 & 26, left panels). Cells that express Nipsnap1-CTF displayed a reduction in all bacterial proteins.

The expected size for the GST-CTF Nipsnap1 is 40 kDa. However, both Coomassie staining and Western blotting show multiple bands at different sizes. The predominant form of Nipnspa1-CTF is approximately 30 kDa, with much lower amounts of the higher molecular weight forms (~40 kDa and ~55 kDa). These results suggest that Nipsnap1-CTF is not being fully translated during induction. This could be due to non-optimized codon usage in the plasmid, since the construct contained mouse Nipsnap1 cDNA sequence. Higher amounts of full-length Nipsnap1-CTF may be obtained by using a modified cDNA which contains optimized *E. coli* codons.

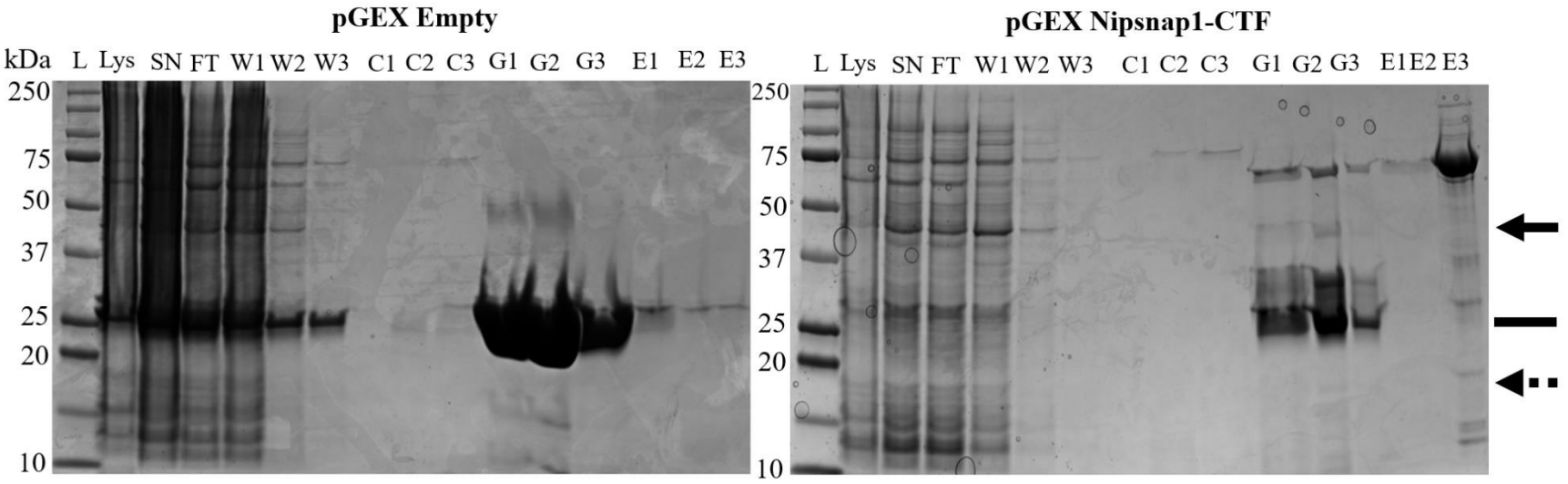

Figure 25. Coomassie staining of samples from purification of supernatants generated from cultures transformed with empty pGEX-4T1 or Nipsnap1-CTF in pGEX-4T1. Wash fractions expected to remove nonspecifically bound proteins are denoted (Wn). Elution fractions after thrombin incubation to promote cleavage of GST-Nipsnap1 are denoted (Cn). Elution fractions after addition of reduced glutathione to the GSTrap column are denoted (Gn). Elution fractions after addition of buffer B2 to remove thrombin from HiTrap column are denoted (En). The solid arrow, solid line, and dashed arrow correspond to approximate locations for GST-Nipsnap1, cleaved GST, and cleaved Nipsnap1, respectively.

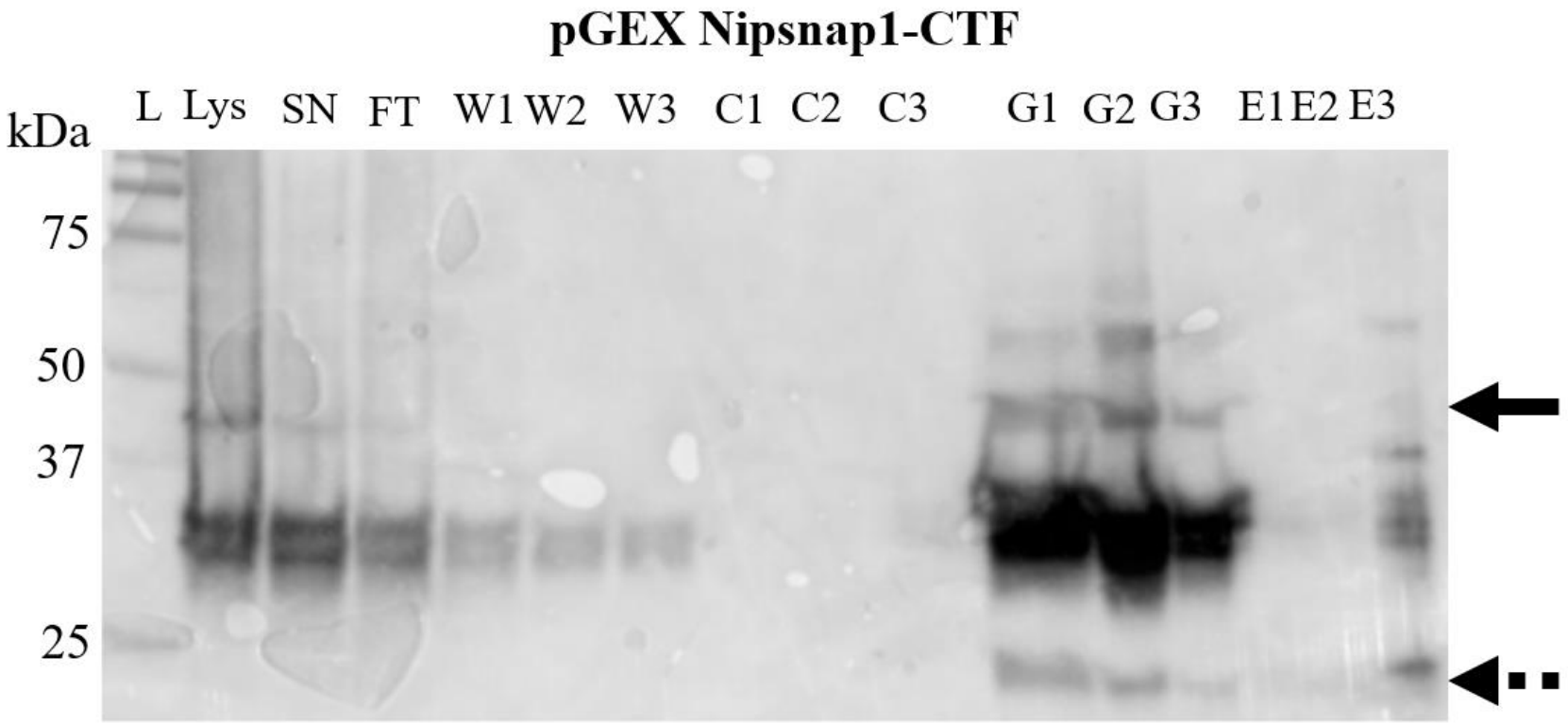

Figure 26. Western blot analysis of samples from purification of supernatants generated from cultures transformed with pGEX-4T1 encoding CTF Nipsnap1. Wash fractions expected to remove nonspecifically bound proteins are denoted (Wn). Fractions expected to elute cleaved protein are denoted (Cn). Fractions expected to remove GST from GSTrap column are denoted (GEn). Fractions expected to remove thrombin from HiTrap column are denoted (Hn). Solid and dashed arrows correspond to expected locations of GST-Nipsnap1 and cleaved Nipsnap1, respectively.

Coomassie staining and Western blot analysis also indicate that cleavage of GST-Nipnsnap1 by thrombin is not occurring efficiently. Thrombin incubation was performed at a range of incubation durations, with trials using fresh thrombin aliquots from multiple shipments (not shown). These results may be due to an inaccessible cleavage site due to the structural conformation of Nipnsap1 protein.

IV - DISCUSSION

The major focus of my study was to optimize conditions for maximal production and purification of recombinant Nipsnap1 proteins. A variety of conditions were evaluated, including culture media composition, induction temperature and time, lysis buffer formulations, sonication procedures, and thrombin digestion time. Even with optimized induction and purification conditions, the expression of Nipsnap1-FL, Nipsnap1-NTF and Nipsnap1-CTF GST fusion proteins were low compared to the GST control.

The low expression of Nipsnap1 protein does not appear to be caused by a bacteriostatic effect (toxicity) of Nipsnap1 or to instability of Nipsnap1 protein. Using growth curve analysis, bacterial growth rates were found to be similar when expressing GST control compared to GST-Nipsnap1 fusion protein. However, expression of GST or GST-Nipsnap1 fusion protein did lower bacterial growth rate compared to uninduced controls. To address the instability issue, a GST fusion expression system was used, whereby Nipsnap1 coding regions were fused in-frame with GST. However, the levels of GST fused Nipsnap1 proteins were still quite low.

Although GST fusion proteins can stabilize some proteins (Kaplan 1997), GST has been demonstrated to be a poor fusion partner for solubility when compared to other common fusion partners, resulting in increased compartmentalization of target protein into inclusion bodies (Hammarström 2002; Hammarström 2006; Dyson 2004; Kohl 2008; Ohana 2009). Due to troubles in solubility with usage of the GST-fusion strategy, other fusion partners that result in higher solubility while maintaining protein stability when

compared to GST may be desirable as a fusion partner for future Nipsnap1 expression and purification efforts. A wide variety of fusion proteins exists for heterologous protein expression in *E. coli* that increase solubility and aid in protein purification (Costa 2014). Newer fusion systems such as the SUMO (Butt 2005), Halo (Ohana 2009), SNUT (Caswell 2010), expressivity tag (Hansted 2011), or Fh8 (Costa 2013) may yield greater amounts of stable, soluble Nipsnap1 for use in a variety of downstream assays to study its biochemical function.

In order to increase the yield of purified Nipsnap1 proteins, large-scale experiments were performed. The majority of purified Nipsnap1 existed in truncated forms. This is likely due to different codon usage in mammalian cDNAs compared to bacteria, which is known to decrease heterologous protein expression in *E. coli* (Gustafsson 2004; Rosano 2009). Optimization of the codons to better accommodate those preferred by *E. coli* (Sharp 1988) may lead to a substantial increase in heterologous protein expression. Additionally, certain *E. coli* cell lines exist that are engineered to contain additional copies of genes that code for tRNAs that reduce expression of heterologous proteins, including BL21-CodonPlus (Agilent Technologies), allowing higher-level expression of genes that are expressed poorly in conventional BL21 strains.

Figure 27 shows the mouse Nipsnap1 cDNA sequence used to generate full-length Nipsnap1 and the corresponding primary amino acid sequence. We found 31 codons out of a total of 284 (11%) that may cause translational problems in *E. coli* as reported in literature (Chen 2006). Notably, 19 out of the 31 (61%) problematic codons were enriched in the C-terminal portion of Nipsnap1. A premature truncation at position 560, where two consecutive unoptimized codons are found, would result in a GST-

Nipsnap1-C truncation protein with a hypothetical molecular weight of roughly 31 kDa, consistent with the primary form of expressed Nipsnap1found during purification (Figure 26). If codon optimization is pursued in future work, the highlighted sequences of Nipsnap1 cDNA found in Figure 27 would likely give the most benefit to heterologous Nipsnap1 expression when altered.

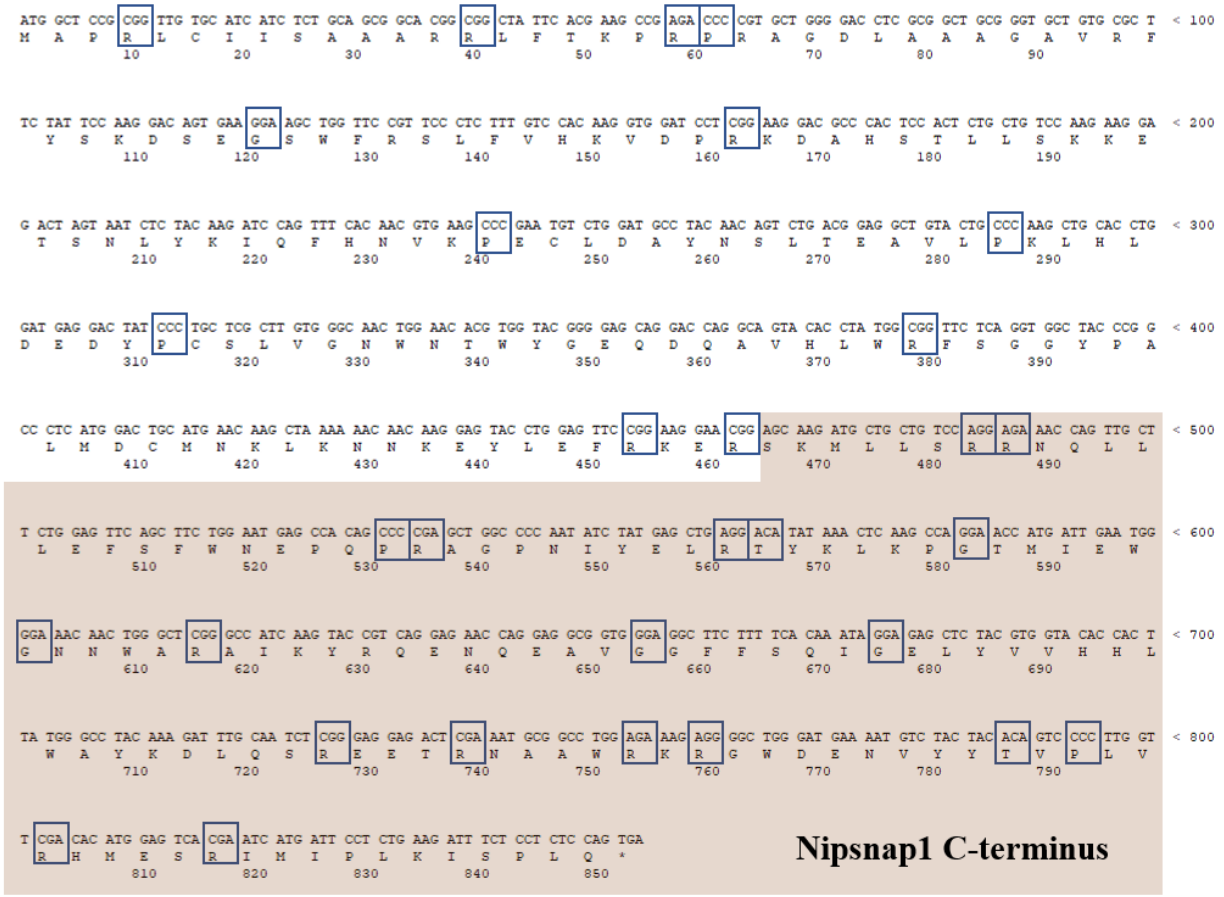

Figure 27. Nipsnap1 cDNA sequence used to generate full-length Nipsnap1. Codons that may cause translational problems due to insufficient tRNA in *E. coli* are highlighted. A significant number (61%) of potentially problematic codons are found within the C-terminus of Nipsnap1. These areas would likely contribute the greatest benefit to successful overexpression if mutagenesis was performed to accommodate more common codon usage in *E. coli*.

Initial CD spectroscopy experimentation demonstrated that Nipsnap-FL can directly bind to NAD+ (Figure 17). CD spectroscopy is a valuable technique for the analysis of protein features in solution and can be used to observe conformational changes of a protein in the presence of ligand (Kelly 2005). Measurements can be carried out rapidly (<30 min) and conveniently. Protein crystallization is not required for analysis, and generally samples utilized in CD experimentation can be recovered and used in further assays due to the methods non-destructive nature. However, there are several limitations to CD spectroscopy (Kelly 2000). CD provides low resolution structural information, and by itself fails to give detailed information about a protein's tertiary or quaternary structure. Tertiary information is found in the near UV (350-250 nm) spectral region, where signals of interest are primarily produced by the chromophores found in aromatic amino acid side chains (320-260 nm) and disulfide bonds (weak, broad absorption bands around 260 nm). Proteins lacking sufficient amounts of amino acids with the above chromophores will fare poorly in CD experimentation.

Isothermal calorimetry (ITC) is a technique that may result in a more definitive validation of Nipsnap1-NAD+ binding. ITC is a powerful technique that can resolve the enthalpic and entropic components of binding affinity (Leavitt 2001). ITC can additionally be used a tool to validate computational structure-based predictions of binding energetics, and allow for accurate structure/energy correlations. Analysis of the Nipsnap1-NAD+ interaction by ITC would allow direct measurement of the energy associated with NAD+ binding to Nipsnap1. A high concentration of purified Nipsnap1 would be desired for ITC experimentation.

Taken together, my results support the hypothesis that Nipsnap1 interacts with NAD+ because CD spectroscopy revealed a tertiary protein structure change in Nipsnap1 when NAD+ was present. However, additional experiment and additional controls are needed to determine the binding affinity of NAD+ (and NADP+) to Nipsnap1. Although several different procedures were tested for optimization of Nipsnap1 expression, none were effective at producing large amounts of recombinant Nipsnap1 protein. I also demonstrated that Nipsnap1 overexpression did not cause a bacteriostatic effect in bacteria. A method for overexpression and purification of large amounts of Nipsnap1 protein has yet to be developed. Future work pursuing this goal using a bacterial expression system should focus on using an *E. coli* optimized Nipsnap1 cDNA construct and the modified induction and solubilization methods developed in this study. Such a system would be invaluable in elucidating Nipsnap1 function, allowing evaluation of protein structure and function in a number of assays that rely on high quantities of purified protein.

REFERENCES

NIH (2017, May 16). *What Happens to the Brain in Alzheimer's Disease?* Retrieved from https://www.nia.nih.gov/health/what-happens-brain-alzheimers-disease

Alzheimer's Association (2018, June 13). *Tests of Alzheimer's & Dementia*. Retrieved from https://www.alz.org/alzheimers-dementia/diagnosis/medical_tests

Barker WW, Luis CA, Kashuba A, Luis M, Harwood DG, Loewenstein D, et al. (2002). Relative frequencies of Alzheimer's disease, Lewy body, vascular and frontotemporal dementia, and hippocampal sclerosis in the State of Florida Brain Bank. *Alzheimer Dis Assoc Disord, 16*(4):203-12.

Burman HM, Westbrook J, Feng Z, Gilliland G, Bhat TN, Weissig H, Shindyalov IN, Bourne PE (2000). The Protein Data Bank. *Nucleic Acids Research, 28*: 235-242.

United States Census Bureau. *2014 National Population Projections*. Retrieved from https://www.census.gov/data/datasets/2014/demo/popproj/2014-popproj.html.

Butt TR, Edavettal SC, Hall JP, Mattern MR. (2005). SUMO fusion technology for difficult-to-express proteins. *Protein Expr. Purif.,* 43, 1–9.

Casper Zweig AS, Villarreal C, Tyner C, Speir ML, Rosenbloom KR, Raney BJ, Lee CM, Lee BT, Karolchik D, Hinrichs AS, Haeussler M, Guruvadoo L, Navarro Gonzalez J, Gibson D, Fiddes IT, Eisenhart C, Diekhans M, Clawson H, Barber GP. (2018). The UCSC Genome Browser database: 2018 update. *Nucleic Acids Res,* D762-D769.

Caswell J, Snoddy P, McMeel D, Buick RJ, Scott CJ. (2010). Production of recombinant proteins in Escherichia coli using an N-terminal tag derived from sortase. *Protein Expr. Purif., 70*, 143–150.

Chen D, Texada D. (2006). Low-usage codons and rare codons of Escherichia coli. *Gene Ther Mol Biol.* 10:1-12.

Citron Oltersdorf T, Haass C, McConlogue L, Hung AY, Seubert P, Vigo-Pelfrey C, Lieberburg I, Selkoe DJ. (1992). Mutation of the beta-amyloid precursor protein in familial Alzheimer's disease increases beta-protein production. *Nature, 360*(6405):672-4.

Claros MG. (1995). MitoProt, a Macintosh application for studying mitochondrial proteins. *Comput Appl Biosci., 11*(4):441-7.

Costa S, Almeida A, Castro A, Domingues L. (2014). Fusion tags for protein solubility, purification and immunogenicity in Escherichia coli: the novel Fh8 system. *Front. Microbiol.,* 5:63.

Costa SJ, Silva P, Almedia A, Conceição A, Domingues L, Castro A. (2013). A novel adjuvant-free H fusion system for the production of recombinant immunogens in Escherichia coli: its application to a 12 kDa antigen from Cryptosporidium parvum. *Bioengineered*, 4, 1–7.

Dvorak P, Chrast L, Nikel P, Fedr R, Soucek K, Sedlackova M, Chaloupkova R, de Lorenzo V, Prokop Z, Damborsky J. (2015). Exacerbation of substrate toxicity by IPTG in Escherichia coli BL21(DE3) carrying a synthetic metabolic pathway. *Microbial Cell Factories,* 14:201.

Dyson MR, Shadbolt SP, Vincent KJ, Perera RL, McCafferty J. (2004). Production of soluble mammalian proteins in Escherichia coli: identification of protein features that correlate with successful expression. *BMC Biotechnol,* 14;4-32.

Eberhardt RY, Eddy SR, Mistry J, Mitchell AL, Potter SC, Punta M, Qureshi M, Sangrador-Vegas A, Salazar GA, Tate J, Bateman A. (2016). The Pfam protein families database: towards a more sustainable future. *Nucleic Acids Research*. 44:D279-D285

Ehlers, M. (2003). Activity level controls postsynaptic composition and signaling via the ubiquitin-proteasome system. *Nat. Neurosci.,* 6, 231–242.

The GTEx Consortium. (2013). The Genotype-Tissue Expression (GTEx) project. *Nat Genet. 45*(6): 580–585.

Ghoshal S, Jones L, Homayouni R. (2014). NIPSNAP1 deficient mice exhibit altered liver amino acid, lipid and nucleotide metabolism. *Metabolomics*, 10, 250–258.

Goelet P, Castellucci VF, Schacher S, Kandel ER. (1986). The long and the short of long-term memory–a molecular framework. *Nature*, 322, 419–422.

Goujon M, McWilliam H, Li W, Valentin F, Squizzato S, Paern J, Lopez R. (2010). A new bioinformatics analysis tools framework at EMBL-EBI. *Nucleic Acids Research,* 38:W695-699.

Gustafsson C, Govindarajan S, Minshull J. (2004). Codon bias and heterologous protein expression. *Trends in Biotechnology*, *22*(7): 346-353.

Hammarström Hellgren N, van Den Berg S, Berglund H, Härd T. (2002). Rapid screening for improved solubility of small human proteins produced as fusion proteins in Escherichia coli. *Protein Sci, 11*(2):313-21.

Hammarström M, Woestenenk EA, Hellgren N, Härd T, Berglund H. (2006). Effect of N-terminal solubility enhancing fusion proteins on yield of purified target protein. *J Struct Funct Genomics, 7*(1):1-14.

Hansted JG, Pietikäinen L, Hög F, Sperling-Petersen HU, Mortensen KK. (2011). Expressivity tag: a novel tool for increasede xpression in Eschericia coli. *J Biotechnol,* 155, 275–283.

He W, Goodkind D, Kowal P. (2016). International Population Reports, P95/16-1, An Aging World. Washington, DC: Government Publishing Office.

Heber S, Herms J, Gajic V, Hainfellner J, Aguzzi A, Rülicke T, von Kretzschmar H, von Koch C, Sisodia S, Tremml P, Lipp HP, Wolfer DP, Müller U. (2000). Mice with combined gene knock-outs reveal essential and partially redundant functions of amyloid precursor protein family members. *J Neurosci, 20*(21):7951-63.

Howe KL, Bolt BJ, Cain S, Chan J, Chen WJ, Davis P, Done J, Down T, Gao S, Grove C et al. (2016). WormBase 2016: expanding to enable helminth genomic research. *Nucleic Acids Res,* (D1):D774-80.

Hunskaar S, Hole K. (1987). The formalin test in mice: dissociation between inflammatory and non-inflammatory pain. *Pain,* 103-114.

Hynes T, Randal M, Kennedy L, Eigenbrot C, Kossiakoff A. (1990). X-ray crystal structure of the protease inhibitor domain of Alzheimer's amyloid beta-protein precursor. *Biochemistry, 29*(43):10018-22.

Islam MM, Nautiyal M, Wynn RM, Mobley JA, Chuang DT, Hutson SM. (2010). Branched-chain amino acid metabolon: interaction of glutamate dehydrogenase with the mitochondrial branched-chain aminotransferase (BCATm*). J Biol Chem,* 285:265-276.

Kaplan W, Husler P, Klump H, Erhardt J, Sluiscremer N, Dirr H. (1997). Conformational stability of pGEX-expressed Schistosoma japonicum glutathione S-transferase: a detoxification enzyme and fusion-protein affinity tag. *Protein Sci, 6*(2):399-406.

Kelly SM, Jess TJ, Price NC. (2005). How to study proteins by circular dichroism. *Biochim Biophys Acta, 1751*(2):119-39.

Kelly SM, Price NC. (2000). The Use of Circular Dichroism in the Investigation of Protein Structure and. *Current Protein and Peptide Science,* 1, 349-384.

Kim CH, Kim S, Seo JH, Change KA, Yu E, Jeong SJ, Chong YH, Suh YH. (2003). C-terminal fragments of amyloid precursor protein exert neurotoxicity by inducing glycogen synthase kinase 3-beta expression. *FASEB J , 17*(13): 1951-3.

Kohl T, Schmidt C, Wiemann S, Poustka A, Korf U. (2008). Automated production of recombinant human proteins as resource for proteome research. *Proteome Sci,* 6:4.

Leavitt S, Freire E. (2001). Direct measurement of protein binding energetics by isothermal titration calorimetry. *Curr Opin Struct Biol,* (5):560-6.

Loo DT, Pike CJ, Whittemore ER, Walencewicz AF, Cotman CW. (1993). Apoptosis is induced by beta-amyloid in cultured central nervous system neurons. Proc Natl Acad Scie USA, 90(17): 7951-7955.

Mattson MP, Cheng B, Culwell AR, Esch FS, Lieberburg I, Rydel RE. (1993). Evidence for excitoprotective and intraneuronal calcium-regulating roles for secreted forms of the beta-amyloid precursor protein. *Neuron, 10*(2):243-54.

Muller T, Meyer HE, Egensperger R, Marcus K. (2008). The amyloid precursor protein intracelluar domain (AICD) as a modulator of gene expression, apoptosis, and cytoskeletal dynamics-relevance for Alzherimer's disease. *Prog Neuorobiol, 85*(4): p. 393-406.

Murrell J, Farlow M, Ghetti B, Benson MD. (1991). A mutation in the amyloid precursor protein associated with hereditary Alzheimer's disease. *Science, 254*(5028):97-9.

Nagase H, Nakayam K. (2014). The intracellular domain of amyloid precursor protein is a potential therapeutic target in Alzheimer’s disease. *Curr Drug Discov Technol, 11*(4): 243-258.

Nautiyal M, Sweatt AJ, MacKenzie JA, Mark Payne R, Szucs S, Matalon R, Wallin R, Hutson SM. (2010). Neuronal localization of the mitochondrial protein NIPSNAP1 in rat nervous system. *Eur J Neurosci,* 32:560-569.

Ohana RF, E. L. (2009). HaloTag7: a genetically engineered tag that enhances bacterial expression of soluble proteins and improves protein purification. *Protein Expr Purif, 68*(1):110-20.

Ohkawara T, N. H. (2011). The amyloid precursor protein intracellular domain alters gene expression and induces neuron-specific apoptosis. *Gene, 475*(1):1-9.

Okamoto K., Ohashi M., Ohno K., Takeuchi A., Matsuoka E., Fujisato K., Minami T., Ito S., Okuda-Ashitaka E. (2016). Involvement of NIPSNAP1, a neuropeptide nocistatin-interacting protein, in inflammatory pain. *Mol. Pain,* 12. pii.

Okuda-Ashitaka E., Ito S. (2015). Pain regulation by nocistatin-targeting molecules: G protein-coupled-receptor and nocistatin-interacting protein. *Vitam. Horm.*, 97:147-165.

Okuda-Ashitaka E, Minami T, Tsubouchi S, Kiyonari H, Iwamatsu A, Noda T, Handa H, Ito S. (2012). Identification of NIPSNAP1 as a nocistatin-interacting protein involving pain transmission. *J. Biol. Chem.*, Epub 2012 Feb 6.

PDB ID 1VQY. Joint Center for Structural Genomics (2005). Crystal structure of a nipsnap family protein with unknown function (atu5224) from agrobacterium tumefaciens str. c58 at 2.40 A resolution.

PDB ID 1VQS. Joint Center for Structural Genomics (2005). Crystal structure of a nipsnap family protein with unknown function (atu4242) from agrobacterium tumefaciens str. c58 at 1.50 A resolution.

Pimplikar S, Nixon RA, Robakis NK, Shen J, Tsai LH. (2010). Amyloid-independent mechanisms in Alzherimer's disease pathogenesis. *J Neurosci, 30*(45): p. 14946-54.

Reitz C, Brayne C, Mayeux R. (2011). Epidemiology of Alzheimer's Disease. *Nat Rev Neurol, 7*(3): 137-152.

Rosano GL, Ceccarelli EA (2009). Rare codon content affects the solubility of recombinant proteins in a codon bias-adjusted Escherichia coli strain. *Microb Cell Fact.,* 8: 41.

Roy A, Kucukural A, Zhang Y. (2010). I-TASSER: a unified platform for automated protein structure and function prediction. *Nature Protocols,* 5: 725-738.

Mondin, R, B. J.-S. (2002). The Effect of Glucose, Lactose, and Galactose on the Induction of β-Galactosidase in E. coli. *Journal of Experimental Microbiology and Immunology*, 2:22-26.

Satoh, K, Takeuchi M, Oda Y, Deguchi-Tawarada M, Sakamoto Y, Matsubara K, Nagasu T, Takai Y. (2002). Identification of activity-regulated proteins in the postsynaptic density. *Genes to Cells,* 7, 187-197.

Schoeber J, Topala C, Lee K, Lambers T, Ricard G, van Der Kemp A, Huynen M, Hoenderop J, Bindels R. (2008). Identification of Nipsnap1 as a novel auxiliary protein inhibiting TRPV6 activity. *Eur J Physiol,* 457:91-101.

Selkoe, E. P. (2002). Deciphering the genetic basis of Alzheimer's disease. *Annu Rev Genomics Hum Genet,* 3:67-99.

Seroussi, E. P. (1998). Characterization of the human NIPSNAP1 gene from 22q12: a member of a novel gene family. *Gene,* 13-20.

Sharp PM, Cowe E, Higgins DG, Shields DC, Wolfe KH, Wright F. (1988). Codon usage patterns in Escherichia coli, Bacillus subtilis, Saccharomyces cerevisiae, Schizosaccharomyces pombe, Drosophila melanogaster and Homo sapiens; a review of the considerable within-species diversity. *Nucleic Acids Res., 16*(17):8207-11.

Sievers F, Wilm A, Dineen D, Gibson T, Karplus K, Li W, Lopez R, McWilliams H, Remmert M, Soding J, Thompson J, Higgins D. (2011). Fast, scalable generation of high-quality protein multiple sequence alignments using Clustal Omega. *Molecular Systems Biology*, 7:539.

Smith DB, Johnson KS. (1988). Single-step purification of polypeptides expressed in Escherichia coli as fusions with glutathione S-transferase. *Gene, 67*(1):31-40.

Stathopulos PB, Scholz GA, Hwang YM, Rumfeldt JA, Lepock JR, Meiering EM. (2004). Sonication of proteins causes formation of aggregates that resemble amyloid. *Protein Sci*, 11:3017-27.

Sulston J, Thomas K, Wilson R, Hillier L, Staden R, Halloran N, Green P, Thierry-Mieg J, Qiu L, et al. (1992). The C. elegans genome sequencing project: a beginning. *Nature, 356*(6364):37-41.

Takata A, Kakiuchi C, Ishiwata M, Kanba S, Kato T. (2010). Behavioral and gene expression analyses in heterozygous XBP1 knockout mice: Possible contribution of chromosome 11qA1 locus to prepulse inhibition. *Neurosci Res, 68*(3): 250-255.

Tummala H, Li C, Homayouni R. (2010). Interaction of a novel mitochondrial protein, 4-nitrophenylphosphatase domain and non-neuronal SNAP25-like protein homolog 1 (NIPSNAP1), with the amyloid precursor protein family. *Eur J Neurosci, 31*(11):1926-34.

Wang JZ, Xia YY, Grundke-Iqbal I, Iqbal K. (2013). Abnormal hyperphosphorylation of tau: sites, regulation, and molecular mechanism of neurofibrillary degeneration. *J Alzheimers Dis,* 33 Suppl 1:S123-39.

Williams DC, V. F. (1982). Cytoplasmic inclusion bodies in Escherichia coli producing biosynthetic human insulin proteins. *Science, 215*(4533):687-9.

Wilson RS, Van Frank RM, Muth WL, Burnett JP. (2012). The natural history of cognitive decline in Alzheimer's disease. *Psychol Aging, 27*(4):1008-17.

Yang J, Yan R, Roy A, Xu D, Poisson J, Zhang Y. (2015). The I-TASSER Suite: Protein structure and function prediction. *Nature Methods,* 12: 7-8.

Yongjin Z, e. a. (2011). Determining the Extremes of the Cellular NAD(H) Level by Using an Escherichia coli NAD-Auxotrophic Mutant. *APPLIED AND ENVIRONMENTAL MICROBIOLOGY,* 6133–6140.

Younge-Pearse T, Chen, AC, Chang, R, Marquez, C, Selkoe, D. (2008). Secreted APP regulates the function of full-length APP in neurite outgrowth through interaction with integrin beta I. *Neural Development, 3*(15).

Zhang Y. (2008) I-TASSER server for protein 3D structure prediction. *BMC Bioinformatics,* 9:40.

Zhang YW, Thompson R, Zhang H, Xu H. (2011). APP processing in Alzheimer's disease. *Mol Brain* 4, 3.

Zhou H, Skolnick J. (2013). FINDSITE(comb): a threading/structure-based, proteomic-scale virtual ligand screening approach. *J Chem Inf Model*, *53*(1):230-40.

APPENDIX

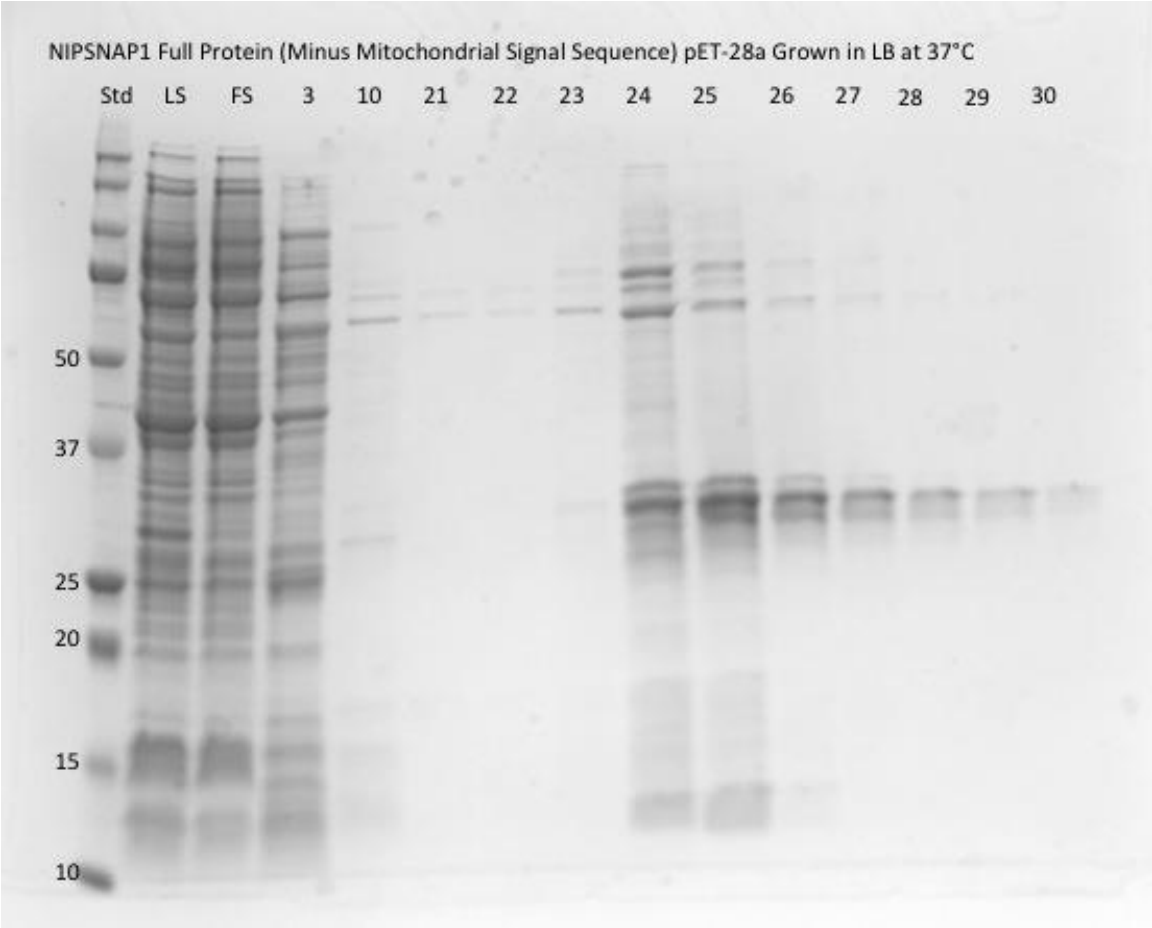

Figure A1. Coomassie stain of the pET-28a-based recombinant Nipsnap1 purification strategy (Gacasan, unpublished). The His-tagged Nipsnap1 protein (30kDa) was purified using Ni-Affinity chromatography. Supernatant was cycled onto a 1 mL Ni sepharose HisTrap HP column (GE Health Sciences) for 1-2 hours at 40 °C, using a peristaltic pump, to ensure maximum protein binding. The column was then washed with buffer A for 20 min, to remove any nonspecifically bound protein, and the bound protein eluted with buffer B (20mM $NaPO_4$, 0.5M NaCl, and 500mM imidazole, pH 7.4).

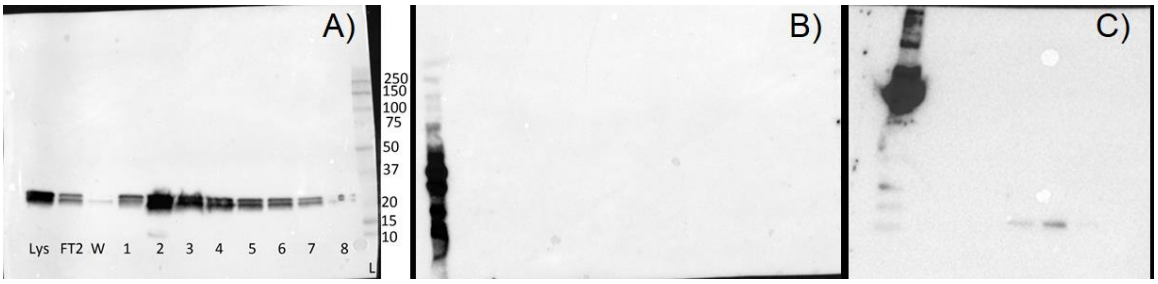

Figure A2. Immunoblot analysis pET28-a recombinant Nipsnap1 protein. Truncated recombinant Nipsnap1 forms were probed with an αHis6 antibody as opposed to our generated αNS1 antibody due to not containing the complete antibody epitope sequence (Epitope = NKLKNNKEYLEFRKER). A) Full-length recombinant Nipsnap1 (30 kDa) was probed with 1:4000 αNS1 generated in our lab and 1:5000 αgoat. Of interest to note is the dual banding of purified recombinant protein. B) N-terminal fragment recombinant Nipsnap1 was probed with 1:1000 αHis6 antibody and 1:5000 αmouse, showing no observed expression. C) C-terminal fragment recombinant Nipsnap1 was probed with1:1000 αHis6 antibody and 1:5000 αmouse. No significant expression is observed.